

**KERNFORSCHUNGSZENTRUM  
KARLSRUHE**

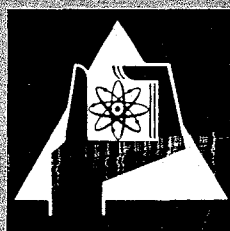
Dezember 1970

KFK 1341

Institut für Angewandte Kernphysik

Analysis of Amorphous and Ion Implanted Layers  
on Silicon by Backscattering and Channeling Effect Measurements

O. Meyer, J. W. Mayer, J. Gyulai



GESELLSCHAFT FÜR KERNFORSCHUNG M. B. H.  
KARLSRUHE



## ANALYSIS OF AMORPHOUS LAYERS ON SILICON BY BACKSCATTERING AND CHANNELING EFFECT MEASUREMENTS<sup>†</sup>

O. MEYER\*, J. GYULAI\*\* and J. W. MAYER

*California Institute of Technology, Pasadena, California 91109, U.S.A.*

Received 21 January 1970

Backscattering and channeling of MeV <sup>4</sup>He ions in single crystals covered with amorphous layers are discussed with the particular purpose of employing this nondestructive method to determine depth dependence of the composition, density and the total thickness of such layers. The analysis shows that the ratio of concentrations (and a relative depth scale) can be found directly from the experimental curves. To determine the absolute concentrations and depth scale independent measurement of stopping powers or layer thickness is required. Oxide layers grown on single crystal Si were used to verify the analytical results and, furthermore, we show illustrative analyses for samples with unknown characteristics. This technique may be applied rather extensively to the analysis of thin films.

### 1. Introduction

In this paper we discuss the application of backscattering and channeling effect measurements to the analysis of amorphous layers, in particular, silicon-oxide layers on silicon surfaces. This technique lends itself readily to analysis of 300 to 2000 Å thick amorphous layers, such as the dielectric layers used for passivation in device technology. Backscattering of charged particles produced in accelerators is a well-known method used for the analysis of surfaces<sup>1-3</sup>). Backscattering of He<sup>+</sup> particles produced in radioactive sources, for example, was applied for the chemical analysis of the lunar surface<sup>4, 5</sup>). The <sup>4</sup>He ions beam generated in an accelerator has the advantage of far higher source strength to beam resolution ratio. This makes it possible to look at small solid angles of the backscattered particles so that the energy spread caused by kinetics is small compared with the energy resolution of the detecting system. We have combined this advantage with directional effects which occur when the incident beam is aligned with the single crystal silicon

\* Permanent address: Institut für Angewandte Kernphysik, Kernforschungszentrum, Karlsruhe, Germany.

\*\* Permanent address: Institut of Experimental Physics, University of Szeged, Hungary.

† Work supported in part by A.F. Cambridge Research Laboratories; 3 MeV accelerator in part by NSF GP-9114 and Nonr-220(47).

underlying the amorphous layer (channeling effect). The background is considerably reduced and also the composition near the interface can be studied in more detail. These techniques have been used to analyze ion-implanted layers<sup>6,7</sup>).

The present paper discusses the application of the combined techniques to the analysis of as-grown oxide layers of about 1000 Å thickness. The experiments indicate the method has some advantage compared with, e.g., weighing<sup>8</sup>) and selective etching techniques<sup>9</sup>) used up to now, as it is non-destructive and also gives the depth distribution of the composition and density. In comparison with the use of nuclear reactions that have been applied, for example, to the study of oxygen diffusion<sup>10</sup>), the backscattering technique provides a simultaneous determination of *both* oxygen and silicon concentrations.

## 2. Analysis of scattering data

Fig. 1 shows the principle of the scattering process<sup>11</sup>). A mono-energetic beam of <sup>4</sup>He ions (mass  $M_1$ , energy  $E'$ ) enters normal to the target surface

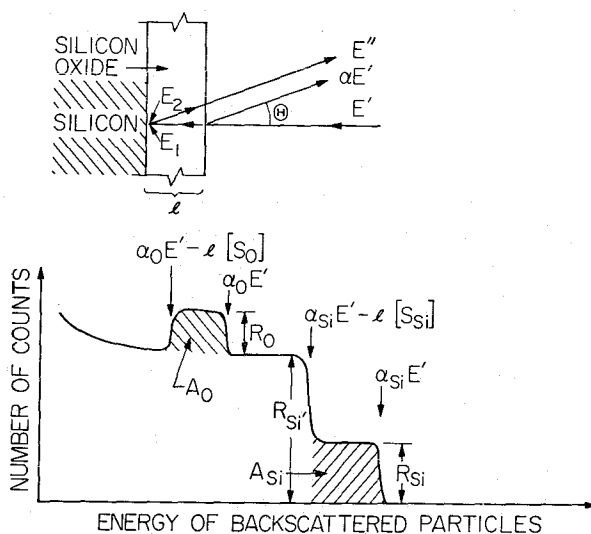


Fig. 1. Schematic illustration of the scattering process and the resulting random spectrum.

(mass  $M_2$ ). The energy of the particles scattered at the surface is  $\alpha E'$ , where  $\alpha$  is the fractional amount of energy after scattering:

$$\alpha = \left\{ \frac{M_1 \cos \theta_L}{M_1 + M_2} + \left[ \left( \frac{M_1 \cos \theta_L}{M_1 + M_2} \right)^2 + \frac{M_2 - M_1}{M_1 + M_2} \right]^{\frac{1}{2}} \right\}^2 \quad (1)$$

Here  $\theta_L$  denotes the scattering angle in laboratory system of coordinates;  $E_1$  is the energy of the particles just before collision after penetrating the surface layer to a depth  $t$ ;  $E_1$  is given by

$$E_1 = E' - \left| \int_0^t \frac{dE}{dx} dx \right|. \quad (2)$$

The energy  $E_2$  immediately after collision is given by

$$E_2 = \alpha E_1, \quad (2a)$$

and  $E''$ , the energy of the outgoing particles as measured with a solid state detector at angle  $\theta$  ( $= 180^\circ - \theta_L$ ) is given by

$$E'' = E_2 - \left| \int_0^t \frac{dE}{dx} \frac{dx}{\cos \theta} \right|, \quad (2b)$$

or inserting eqs. (2a) and (2) in (2b)

$$E'' = \alpha E' - \left| \alpha \int_0^t \frac{dE}{dx} dx \right| - \left| \int_0^t \frac{dE}{dx} \frac{dx}{\cos \theta} \right|. \quad (3)$$

For  $\text{He}^+$  particles incident on oxide films, the values of  $dE/dx$  are  $\lesssim 30 \text{ eV/\AA}$  for all energies involved here. Thus the energy loss of particles traversing the films does not exceed 100 keV and typically is less than 30 keV. Since  $dE/dx$  changes only slowly with energy, average values of  $dE/dx$  can be used for the incoming and outgoing paths respectively. Then

$$E'' \approx \alpha E' - t[S], \quad (4)$$

where we define  $[S]$ , the backscattering energy loss parameter, by

$$[S] \equiv \alpha \left. \frac{dE}{dx} \right|_{E_1} + \frac{1}{\cos \theta} \left. \frac{dE}{dx} \right|_{E_2}. \quad (4a)$$

In this definition  $\bar{E}_1$  and  $\bar{E}_2$  are intermediate energies between  $E'$  and  $E_1$ , and  $E_2$  and  $E''$ , respectively. At the energies used here, where  $t[S] \ll E'$ , one may take  $\bar{E}_1 \simeq E'$  and  $\bar{E}_2 \simeq E_2$  with negligible loss of accuracy. Thus, for the thickness of interest here the energy scale in fig. 1 can be converted to a linear depth scale. For increased film thickness where energy losses along the paths may be large, this linear depth scale will not be maintained unless higher incident beam energies are used.

For the case of an oxide layer on silicon (fig. 1), the energy of particles scattered at the surface from silicon atoms is  $\alpha_{\text{Si}} E'$  and from oxygen  $\alpha_{\text{O}} E'$ . In

the experimental arrangement  $\theta \approx 16^\circ$  shown, the particles backscattered from Si and O are well separated in energy ( $\alpha_{\text{Si}} = 0.57$  and  $\alpha_{\text{O}} = 0.37$ ).

The total energy difference for particles scattered at the surface and particles going through an oxide layer of thickness  $l$  is  $\alpha E' - E'' = l[S]$ , where  $[S] = [S_{\text{O}}]$  for particles scattered from oxygen atoms and  $[S] = [S_{\text{Si}}]$  for particles scattered from silicon. Since  $[S_{\text{O}}]$  is generally not equal to  $[S_{\text{Si}}]$  the depth scales in the different regions in fig. 1 are not equal. That is, the conversion of energy losses to depth is different in the oxygen peak (shaded area,  $A_{\text{O}}$ ) from that in the silicon "step" (shaded area,  $A_{\text{Si}}$ ). Assuming a sharp interface between the oxide and the underlying silicon and homogeneous distribution of the atoms in the amorphous layers, the above energy difference  $\Delta E$  (energy shift) between particles scattered from silicon atoms at the oxide surface and silicon atoms at the silicon substrate oxide interface is  $l[S_{\text{Si}}]$ , whereas the width (full width at half maximum) of the oxide peak  $HW_{\text{O}}$  is equal to  $l[S_{\text{O}}]$ . That is,

$$\Delta E = l[S_{\text{Si}}] \quad \text{and} \quad HW_{\text{O}} = l[S_{\text{O}}]. \quad (5)$$

Thus, without explicit knowledge of the specific energy losses involved, the measured ratio  $\Delta E/HW_{\text{O}}$  can be used to correct for the different depth scales in comparing the same volume elements at a given depth. Note also that  $[S]$  is different for silicon in the oxide layer  $[S_{\text{Si}}]$  and silicon in silicon  $[S_{\text{Si}'}]$ .

The linear response of semiconductor nuclear particle detectors provides a fixed energy per channel  $\delta E$  in the multichannel analyzer. The scattering yield  $R'(E) \delta E$  (i.e., the number of backscattered particles having energies between  $E$  and  $E + \delta E$ ) from a zone of width  $\delta t$  corresponding to one channel at depth  $t$  is

$$R'(E) \delta E = N_{\text{T}}(t) \sigma f \delta t, \quad (6)$$

where  $\delta t$  is given by  $\delta E/[S]$  and  $N_{\text{T}}$  is the density of the target atoms at depth  $t$ . For convenience we use  $\sigma \cdot f$  to denote  $[(d\sigma/d\Omega)\Omega]_{\text{L}}$ , the Rutherford cross section formula and solid angle of the scattering in the laboratory system of coordinates. Factor  $f$  stands for the geometry of the experimental set up. From eq. (6) the absolute concentration of oxygen and silicon atoms can be determined:

$$N_{\text{O}}(t) = R'_{\text{O}}(E) [S_{\text{O}}]/\sigma_{\text{O}} \cdot f \quad \text{and} \quad N_{\text{Si}}(t) = R'_{\text{Si}}(E) [S_{\text{Si}}]/\sigma_{\text{Si}} \cdot f. \quad (7)$$

The concentration ratio at any depth  $t$  is given by:

$$\frac{N_{\text{O}}(t)}{N_{\text{Si}}(t)} = \frac{R_{\text{O}}(E) [S_{\text{O}}] \sigma_{\text{Si}}}{R_{\text{Si}}(E) [S_{\text{Si}}] \sigma_{\text{O}}}, \quad (8)$$

where  $R = R' \delta E$  denoted the number of counts per channel.

Again, note that for a sharp interface and an approximately homogeneous layer the ratio  $[S_O]/[S_{Si}]$  is equal to  $HW_O/\Delta E$ . Thus, although determination of the absolute concentrations requires knowledge of  $[S]$  and  $f$ , eq. (7), the ratio of the concentrations can be found directly from analysis of the energy spectra of backscattered particles using measured values of  $HW_O/\Delta E$  and calculated values of  $\sigma_{Si}/\sigma_O$  (here,  $\sigma_{Si}/\sigma_O = 3.08$ ). If the thickness of the layer is known, the  $[S]$  values and the absolute depth scale can be given.

For amorphous layers of known thickness, the concentrations can also be calculated from the backscattering yield  $R_{Si}$  from the underlying substrate. The "step" in the energy spectra at  $\alpha_{Si}E' - I[S_{Si}]$  in fig. 1 reflects the difference between the concentration of Si atoms in the oxide layer ( $N_{Si}$ ) and underlying silicon ( $N_{Si'}$ ) as well as the difference in  $[S]$  values in the two regions. The ratio of  $N_{Si}$  to the concentration of silicon atoms in the substrate  $N_{Si'}$  is

$$\frac{N_{Si}}{N_{Si'}} = \frac{R_{Si} [S_{Si}]}{R_{Si'} [S_{Si'}]}, \quad (9)$$

where  $R_{Si'}$  is the number of counts per channel produced by particles scattered from the Si substrate near the interface. From eq. (9)  $N_{Si}$  can be determined by using the specific energy losses  $dE/dx$  for  $\alpha$ -particles in Si to calculate  $[S_{Si'}]$ . These specific energy losses are difficult to measure and are known within an error of about 10%<sup>12</sup>).

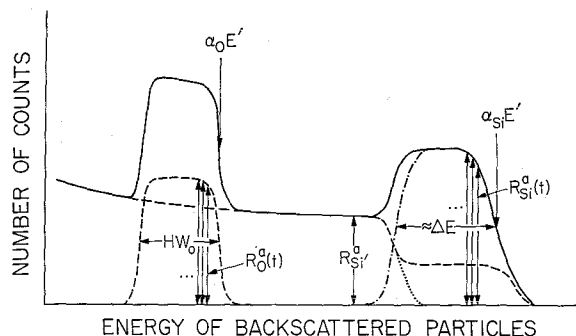


Fig. 2. Schematic drawing of the aligned spectra. In this case the incident beam is aligned with an axis of the underlying silicon. The yield from the amorphous layer is not affected.

Fig. 2 is a schematic drawing of aligned spectra, where the incident beam is aligned with a crystal axis. Compared to the random spectra, the contribution from the substrate is strongly reduced, which permits more accurate determination of the oxygen concentration. The height of the aligned

spectrum  $R_{Si}^a$ , is due to dechanneling arising from increased divergence of the beam as it passes through the oxide layer and hence its magnitude depends on  $E'$ , on the orientation of the underlying Si with the beam, and on the total oxide thickness. For a given thickness the amount of dechanneling can be reduced by using higher energies or choosing the  $\langle 110 \rangle$  orientation. Higher energies are often desirable to decrease the influence of the dechanneled spectrum in the analysis of the oxygen peak. The height of the aligned spectrum  $R_{Si}^a$  can also be reduced still further by use of double alignment (or uniaxial channeling) techniques<sup>13</sup>). These considerations become an important factor in the analysis of amorphous layers on higher  $Z$  substrates (such as GaAs) where the random spectrum is higher due to the  $Z^2$  dependence of the cross-section.

The analysis of the aligned spectra in the region corresponding to the interface between the silicon and oxide layer depends somewhat on the nature of the interface. Assuming a sharp interface as a first approximation, one can normalize  $R_{Si}$  (from the random spectrum) to  $R_{Si}^a$  of the aligned spectrum in order to separate the contribution of the surface layer from that of the bulk. The extrapolated dotted line in fig. 2 represents the silicon

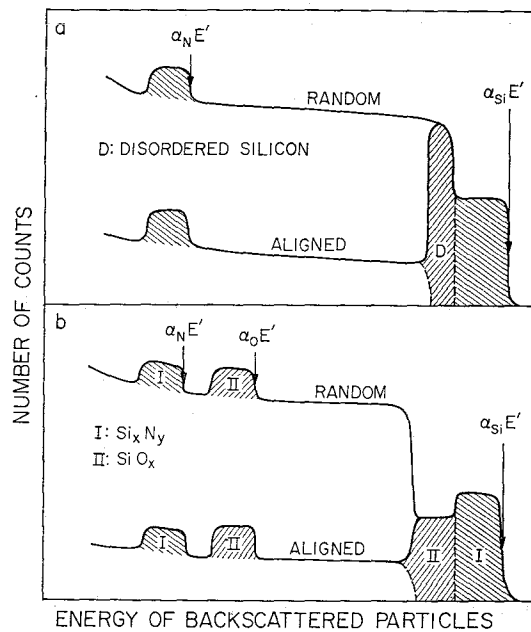


Fig. 3. Schematic random and aligned spectra for silicon samples with (a) an amorphous silicon layer between the silicon and nitride layer and (b) a nitride layer deposited on an oxide layer.

surface shifted by an amount of  $\Delta E$ . This line, together with the adjoining portion of the normalized random spectrum (dashed line) were then used to correct the surface peak. The width of the corrected surfaced peak should then coincide with the energy shift  $\Delta E$ .

In any specific case, this assumption can be tested by gradually etching the oxide layer and thus reducing the value of  $R_{Si}^a$ . The calculated distribution of Si in the oxide layer near the interface should remain unchanged as the layer thickness is reduced.

Some applications of the analysis method are shown schematically in fig. 3. The case where a heavily disordered (amorphous) silicon layer lies beneath a nitride layer is shown in fig. 3a. Here the contribution from the amorphous layer is most evident in the aligned spectrum, region D in fig. 3a. The study of the interface between the disordered layer and the single crystal silicon is limited to a certain extent by the ambiguities in the correction involved (dashed line in fig. 3a). An experimental case of this nature has been discussed in evaluation of nitride layers on silicon<sup>14</sup>). A similar situation would also be found in implantation studies where an amorphous layer is formed by implanting through an oxide layer.

Fig. 3b shows the spectra that would be found on a double layer of dielectric on silicon – here a nitride layer deposited on a previously formed oxide layer. This type of structure is commonly used in integrated circuit technology and samples have been analyzed by use of the backscattering technique<sup>15</sup>). In the spectra, the oxygen and nitrogen peaks are inverted in the energy scale because  $\alpha_N < \alpha_O$ . The separation between the peaks depends on beam energy and layer thicknesses.

### 3. Experimental technique

Backscattering and channeling effect measurements were made using a 3 MeV accelerator and <sup>4</sup>He ion beam between 1.0 and 2.0 MeV. The energy distribution of backscattering particles was measured with a surface barrier detector. The ultimate depth resolution was set by the energy resolution of the detecting system; it was about 100 to 150 Å for the beam energies and experimental set up used. Details of the experimental arrangement have been described earlier<sup>16</sup>). In order to investigate the validity of eqs. (6) and (7), thermally-grown oxide layers on Si with well-known thickness (measured by ellipsometry) and well-known average composition<sup>8</sup>) were used. Silicon used was single crystal Czochralski pulled, phosphorous doped,  $\langle 111 \rangle$  and  $\langle 110 \rangle$  surface oriented, with a resistivity range of 1.5–2.5 ohm-cm. Oxidation was performed under controlled oxidizing atmosphere in a quartz reaction tube contained in a silicon carbide furnace. To show that the technique was

sensitive to changes, measurements were done on thermal oxide (sample A), anodic oxides (sample B), sputtered oxides (sample C), and oxides formed by deposition from  $\text{SiH}_4$  with  $\text{O}_2$  carrier gas at  $500^\circ\text{C}$  (sample D). Anodization of Si was performed in a solution of N-methylacetamide,  $\text{KNO}_3$  and varying  $\text{H}_2\text{O}$  content.

#### 4. Results and discussion

##### 4.1. SPECTRA

The random and aligned spectra for two incident beam energies are shown in fig. 4 for a  $1540 \text{ \AA}$  thermally grown oxide layer on silicon. The step in the random spectrum near channel 150 reflects the smaller concentration of

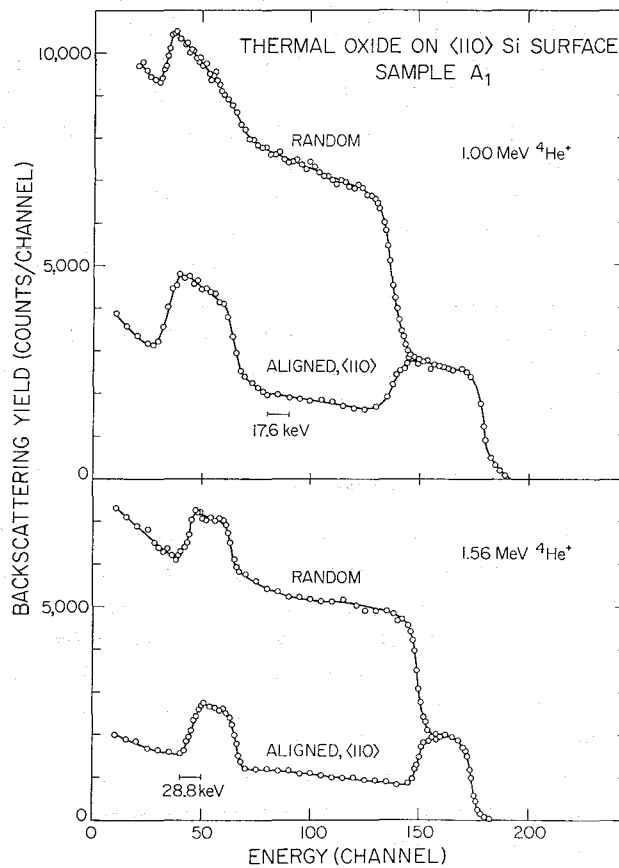


Fig. 4. Random and aligned spectra for 1.00 and 1.56 MeV  $^4\text{He}^+$  ions incident on a  $1540 \text{ \AA}$  thermally grown oxide layer on  $\langle 110 \rangle$  oriented silicon. The energy scales are indicated for the two-beam energies.

silicon atoms in the oxide layer as compared to the underlying silicon substrate. The flat-tops of the surface step and oxide peak (after subtracting the contribution from the underlying Si random spectrum) indicate that there is a nearly uniform distribution of O and Si atoms in the oxide layer. In the aligned spectra, the yield (number of counts per channel) from the underlying Si is strongly reduced, whereas the yields of particles scattered from Si atoms in the amorphous oxide layer are equal in the random and aligned spectra.

#### 4.2. DEPTH SCALE

Fig. 5 shows the spectra for different oxide layer thicknesses. The oxide layer (sample A<sub>2</sub>) was thinned in four steps (original and 2 steps shown in fig. 5) by use of a buffered HF solution. The thickness of the oxide layer after

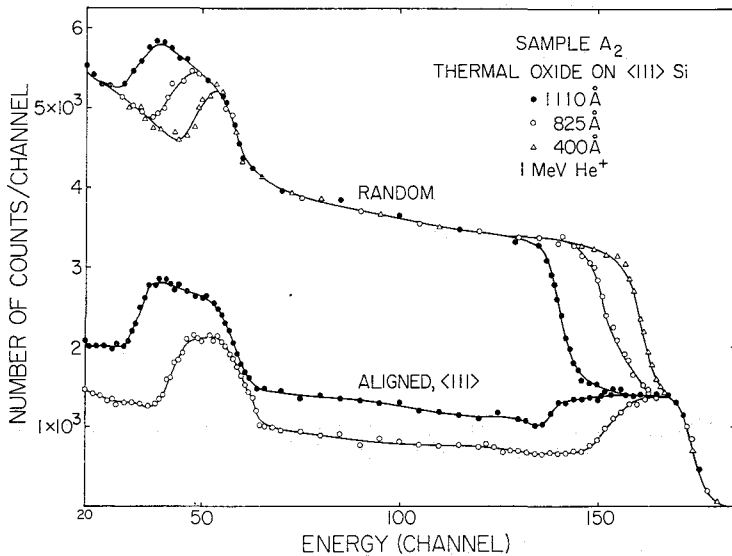


Fig. 5. Random and aligned spectra for 1.00 MeV  $^4\text{He}^+$  ions incident on a 1110 Å thermally grown oxide layer in  $\langle 111 \rangle$  oriented silicon. Also shown are the spectra obtained after the oxide layer was thinned to 825 and 400 Å.

each step was measured by ellipsometry measurements. As indicated in fig. 5, the width\* of the step  $\Delta E$  and of the oxide peak  $HW_0$  decreased with decreasing thickness of oxide layer. Backscattering measurements after

\* We measured  $\Delta E$  as a distance in energy between the points where leading edges of the surface step and the silicon step reached a value of 85% of the random level behind the steps.

each step indicated that  $\Delta E$  and  $HW_O$  were linear functions of oxide thickness. This linear relation is shown in fig. 6 indicating that a sharp interface exists between the silicon and the thermally grown oxide layer. To test further the nature of the interface, a 1000 Å oxide layer was thinned in a buffered HF solution until the number of counts in the oxygen peak was comparable to that in a well-etched silicon sample which had been kept in room ambient for several days. There was some excess amount of displaced Si atoms in the thinned oxide layer corresponding to  $\lesssim 10^{16}$  atoms/cm<sup>2</sup> (approximately twice that in the control sample). These excess Si atoms were

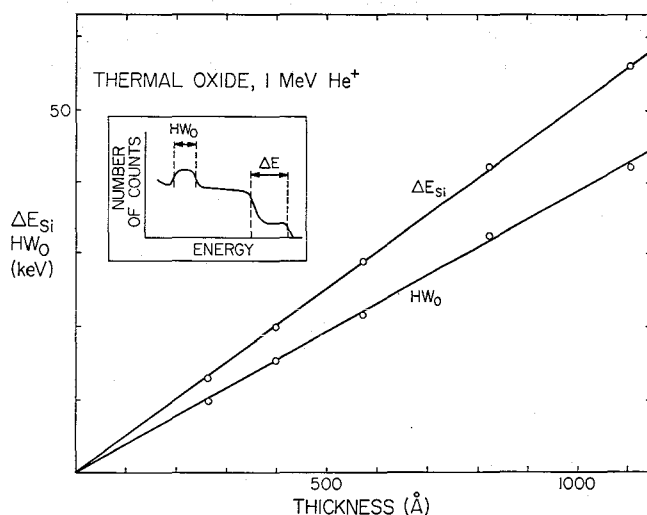


Fig. 6. Measured  $\Delta E$  and  $HW_O$  values versus oxide thickness for beam energy 1.000 MeV. These data were obtained from spectra similar to that shown in fig. 5.

distributed in a layer smaller than the resolution of the detecting system and had only a minor influence in the analysis of thermally grown, 1000 Å oxide layers.

As pointed out previously, if there is a sharp interface between the underlying silicon and the oxide layer, one can replace the ratio  $[S_O]/[S_{Si}]$  in eq. (8) by the measured ratio  $HW_O/\Delta E$ . Values of  $\Delta E$  and  $HW_O$  were determined on thermally-grown oxide layers of thickness between 1000 and 1200 Å. Use of these ratios along with the calculated value of the cross-section ratio  $[\sigma_{Si}/\sigma_O]$  allows determination of the ratio  $N_O/N_{Si}$  as a function of relative depth. The absolute depth scale and hence values of  $[S_O]$  and  $[S_{Si}]$  were found from ellipsometry measurements of the thickness of the

different layers. For  $\theta = 16^\circ$ ,  $[S_O] = 38.5$  and  $41.2$ , and  $[S_{Si}] = 48.3$  and  $49$  for energies of  $1.0$  and  $1.56$  MeV, respectively.

#### 4.3. COMPOSITION

The ratio  $N_O(t)/N_{Si}(t)$  for the 5 thicknesses of the oxide layer on sample  $A_2$  are given in fig. 7. The aligned spectra were used in the analysis. It can be seen that the sample is nearly stoichiometric throughout the oxide thickness (as can also be found in fig. 8 for the thermally-grown oxide, sample  $A_1$ ). Further, in the regions of overlap in the depth distribution, the ratios agree. The errors are about  $\pm 3\%$  and depend primarily on the statistics in the number of counts per channel. The small deviation from stoichiometry at the surface may originate from the fixed depth resolution of the system. Errors in the slope of the drop at the interface originate from both the correction used in the interface region (see fig. 2) and detector resolution.

From knowledge of the  $[S]$  values, the concentrations can be determined within an error of  $10\%$  using specific energy losses of  $^4\text{He}$  particles in silicon. For the thermally-grown oxide layers, the concentration of Si ( $2.2 \times 10^{22}/\text{cm}^3$ ) and oxygen ( $4.45 \times 10^{22}/\text{cm}^3$ ) were in agreement with previously established values. On the other hand one may calculate  $[S_{Si}]$  using density values of well-known stoichiometric thermally-grown oxide layers.

Measurements were performed on samples  $A_1$ , B, C and D, produced by different fabrication procedures. The results of the analysis are shown

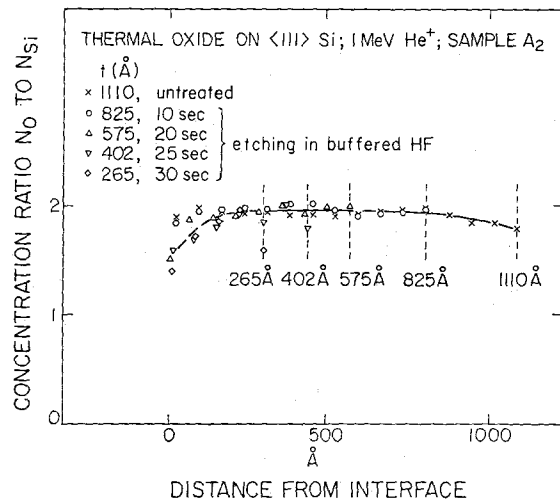


Fig. 7. Distribution of  $N_O/N_{Si}$  for sample  $A_2$  whose thickness had been reduced in four steps by etching. The thickness data are from ellipsometry measurements.

in fig. 8. The thermal oxide (sample A<sub>1</sub>) was found to be stoichiometric over the total oxide thickness, whereas the sputtered oxide (sample C) and the oxide grown from SiH<sub>4</sub> in O<sub>2</sub> atmosphere (sample D) were found to have an average concentration ratio smaller than two.  $N_{\text{O}}/N_{\text{Si}}$  for sample C varies between 1.9 and 1.95 over the total layer thickness. This result is in reasonable agreement with literature values<sup>17</sup>). For anodic oxide the concentration ratio was found to depend on the water content of the electrolyte. 1–2% H<sub>2</sub>O in NMA + KNO<sub>3</sub> resulted in oxides with  $N_{\text{O}}/N_{\text{Si}}$  equal 2. Sample B was produced with water excess (about 10%); a ratio of about 2.15 was found for this sample.

For these samples, the measured ratios of  $\Delta E/HW_{\text{O}}$  were used. However, these values did not deviate appreciably from those for thermally grown

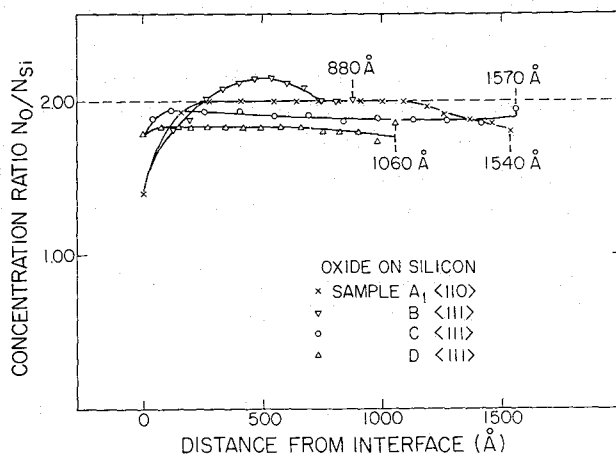


Fig. 8. Distribution of  $N_{\text{O}}/N_{\text{Si}}$  for samples prepared by different oxide growth techniques. Sample A<sub>1</sub>, thermally grown (spectra shown on fig. 4); Sample B, anodic oxide with water excess; Sample C, sputtered oxide, and Sample D, grown from SiH<sub>4</sub> in O<sub>2</sub> atmosphere.

stoichiometric oxide layers. Therefore, thickness determinations were made using the  $[S]$  values given above. In cases where the ratio deviates appreciably from those of stoichiometric samples, an independent measurement of thickness is required.

### 5. Summary

In backscattering measurements of amorphous layers on silicon, information about the concentrations of both oxygen and the silicon in the layer can be determined. The uniformity of the layer can be estimated directly from the shape of the random and aligned spectra.

There are two cases to consider:

a) *Uniform composition.* One can determine  $N_{\text{O}}/N_{\text{Si}}$  and a relative depth scale, from the measured yields and  $\Delta E/HW_{\text{O}}$  ratio [eq. (8)]. To determine the absolute concentration (and depth scale) the layer thickness must be known and either the experimental geometry [factor  $f$  in eq. (7)] or the  $[S]$  values for the substrate material. The concentrations can be determined by comparison with spectra from samples of known composition where  $[S]$  values are known (for example, Si or thermally-grown  $\text{SiO}_2$ ). For oxide layers where the  $\Delta E/HW_{\text{O}}$  ratios do not deviate appreciably from that in stoichiometric oxide layers, the  $[S]$  values given in section 4.2 can be used to determine the concentrations and the thickness.

b) *Non-uniform composition.* For multilayer structures where each layer is uniform in composition, the comments in (a) apply. For single layers where the composition varies strongly with depth, analysis is difficult if  $[S]$  values are depth dependent. The ratio of  $N_{\text{O}}$  to  $N_{\text{Si}}$  can be found from  $\Delta E/HW_{\text{O}}$ , but the depth scale may be distorted. If the thickness is known, an average  $[S]$  value can be used to estimate the concentrations.

We can see from the above that the backscattering technique can be applied rather extensively to the analysis of thin films. For any given film composition, it is preferable to choose the analyzing beam (species and energy) and film thickness so that the energy range for particles back-scattered from different elements do not overlap. For example, MeV He beams are adequate for 300 to 3000 Å thick silicon-oxide and nitride layers on Si or GaAs. The energy difference is large enough so that multilayer oxide-nitride structures can be evaluated.

If the incident beam is aligned with one of the crystal axes of the underlying material, the yield of backscattered particles from the single crystal substrate is reduced. This allows a more accurate determination of the yield from the lower mass elements in the amorphous layer. It also gives information on the amount of disorder (silicon atoms off lattice-sites) near the interface. In some cases layer thinning techniques are required to determine the nature of the interface region.

For crystalline films, such as epitaxial layers, the composition must be determined from the random spectra. The aligned spectra can provide information on the presence of structural defects at the interface and possibly the misalignment between substrate and layer.

For amorphous layers, the spectra obtained when the beam is aligned with the substrate axes are preferable to use in analysis. This is an important consideration for higher  $Z$  substrates such as GaAs where the random yield from the substrate is increased due to the  $Z^2$  dependence of the scattering cross-section.

### Acknowledgements

The authors wish to acknowledge the many discussions with C. A. Barnes about the analysis technique. We are grateful to V. Rodriguez and D. R. Berker who supplied the samples. One of us (J. G.) acknowledges a fellowship from the International Research and Exchanges Board.

### References

- 1) S. Rubin, Nucl. Instr. Methods **5** (1959) 177.
- 2) D. A. Thompson, H. D. Barber and W. D. MacKintosh, Appl. Phys. Letters **14** (1969) 102.
- 3) J. A. Patterson, A. L. Turkevich and E. Franzgrote, J. Geophys. Res. **70** (1965) 1311.
- 4) A. L. Turkevich, Science **134** (1961) 672.
- 5) A. A. Loomis, JPL Tech. Rept. No. 32-606 (April 30, 1964).
- 6) L. Eriksson, J. A. Davies, N. G. E. Johansson and J. W. Mayer, J. Appl. Phys. **40** (1969) 842.
- 7) J. W. Mayer and O. J. Marsh, in: *Applied Solid State Science*, Vol. 1 (Academic Press, New York, 1969) p. 239.
- 8) B. E. Deal, J. Electrochem. Soc. **110** (1963) 528.
- 9) W. A. Pliskin and H. S. Lehman, J. Electrochem. Soc. **112** (1965) 1013.
- 10) See, for example, G. Amsel and D. Samuel, Anal. Chem. **39** (1967) 1689.
- 11) See, for example, D. Powers and W. Whaling, Phys. Rev. **126** (1962) 61.
- 12) C. Williamson and J. T. Boujot, CEA-2189 (1962). Data also given in ORTEC Surface Barriers Manual.
- 13) E. Bøgh, Can. J. Phys. **46** (1968) 651.
- 14) J. Gyulai, O. Meyer, J. W. Mayer and V. Rodriguez, Appl. Phys. Letters. **16** (1970) 232.
- 15) J. Gyulai, O. Meyer and J. W. Mayer, J. Appl. Phys. (August 1970).
- 16) S. T. Picraux, Ph.D. Thesis, California Institute of Technology, 1969.
- 17) W. A. Pliskin, Thin Solid Films **2** (1968) 1.

## ANALYSIS OF Rb AND Cs IMPLANTATIONS IN SILICON BY CHANNELING AND HALL EFFECT MEASUREMENTS\*

O. MEYER† and J. W. MAYER

California Institute of Technology, Pasadena, California 91109

(Received 2 February 1970; in revised form 23 March 1970)

**Abstract**—Analyses of silicon samples implanted with 5–50 keV Rb and Cs ions at substrate temperatures of 350°C and room temperature (R.T.) were made by use of Hall effect and sheet resistivity measurements and channeling techniques. Within limits of detection ( $\leq 10\%$ ) neither Rb nor Cs was found to occupy substitutional or tetrahedral interstitial lattice sites. This behavior seems to be independent of implantation or anneal temperature. Outdiffusion effects were observed for both species. In Hall effect measurements on R.T. implanted samples, the number of carriers/cm<sup>2</sup>,  $N_s$ , exhibited an increase at temperatures significantly above that where the lattice reordered and a decrease below that where outdiffusion started. The maximum value in the average carrier concentration was about  $5 \cdot 10^{18}$ /cm<sup>3</sup> for Rb and  $10^{18}$ /cm<sup>3</sup> for Cs. In almost every respect the behavior of Cs and Rb implanted samples differed from that found for Group II, III, V and VI implanted species.

**Résumé**—On a fait des analyses d'échantillons de silicium implantés d'ions de Rb et de Cs de 5 à 50 keV à des températures de soustrait de 350°C et à température ambiante (R.T.) à l'aide de l'effet Hall, de mesures de résistivité de feuille et de techniques de canalisation. Dans les limites de détection ( $\leq 10\%$ ) ni le Rb ni le Cs ne semblent occuper de sites de treillis interstitial tétrahédrique ou substitutionnel. Ce comportement semble être indépendant de la température d'implantation ou de recuit. Des effets de diffusion externe ont été observés pour les deux genres. Dans les mesures par effet Hall sur des échantillons implantés à température ambiante, le nombre de porteurs/cm<sup>2</sup>,  $N_s$ , révéla un accroissement de température considérablement supérieur à celle où le treillis se réorganise et un décroissement au-dessous de celui où la diffusion externe commence. La valeur maximum dans la concentration de porteur moyenne était d'environ  $5 \cdot 10^{18}$ /cm<sup>3</sup> pour le Rb et  $10^{18}$ /cm<sup>3</sup> pour le Cs. A presque tous points de vue le comportement des échantillons implantés de Rb et de Cs était différent de celui trouvé pour les genres implantés des groupes II, III, V et VI.

**Zusammenfassung**—Mittels Halleffekt, Schichtwiderstandsmessung und einer Channeltechnik wurden Siliziumproben analysiert, die bei einer Substrattemperatur von 350°C und bei Zimmertemperatur durch Rb- und Cs-Ionen mit einer Energie von 5 bis 50 keV dotiert worden waren. Innerhalb der Fehlergrenze für die Beobachtung (kleiner 10 Prozent) wurde kein Cs und Rb auf Gitterplätzen oder in tetraedrischen Zwischengitterplätzen gefunden. Dieses Verhalten scheint unabhängig von der Implantations- und Ausheiltemperatur zu sein. Für beide Ionenarten wurde eine Ausdiffusion beobachtet. Die Hall-Trägerdichte  $N_s$  von Proben, die bei Zimmertemperatur dotiert wurden, zeigt eine Zunahme oberhalb der Ausheiltemperatur des Gitters und eine Abnahme unterhalb der Temperatur für welche die Ausdiffusion einsetzt. Der Maximalwert für die mittlere Trägerdichte lag für Rb bei etwa  $5 \cdot 10^{18}$ /cm<sup>3</sup> und für Cs bei  $1 \cdot 10^{18}$ /cm<sup>3</sup>. In nahezu jeder Hinsicht war das Verhalten der mit Cs und Rb dotierten Proben verschieden gegenüber Proben, die mit Elementen der 2., 3., 5. und 6. Gruppe dotiert waren.

\* Supported in part by A.F. Cambridge Research Laboratories, National Science Foundation [GP-9114] and the Office of Naval Research [Nonr-220(47)].

† Permanent address: Inst. f. Angew. Kernphysik, Kernforschungszentrum, Karlsruhe.

### 1. INTRODUCTION

LATTICE location and electrical behavior of Group II, III, V and VI dopants in Si have been studied in recent years.<sup>(1-3)</sup> Strong correlations were found regarding lattice position within each

group, whereas the electrical results show considerable individual behavior although general trends were found within each group.

In this study we chose Group I elements (Rb and Cs) because the early investigations of the electrical characteristics of implanted species (other than Group III and V dopants) were concerned with this group. McCALDIN *et al.*<sup>(4-6)</sup> demonstrated that donor centers at concentrations of about  $10^{19}/\text{cm}^3$  could be introduced into Si by implanting  $\text{Cs}^+$  or  $\text{Na}^+$ , and it was suggested that these centers corresponded to interstitial alkali ions. These measurements were primarily obtained from sheet resistance and capacitance-voltage characteristics of the implanted *p-n* junctions.

The purpose of this investigation was to use backscattering and channeling techniques together with Hall effect measurements to determine if the Group I atoms did occupy tetrahedral interstitial lattice positions and if their electrical behavior could be correlated with lattice location. We investigated Rb and Cs because these elements had sufficiently higher masses than that of Si, so that the MeV  $^4\text{He}$  ions backscattered from these impurities could be well separated in energy from those scattered from the Si lattice. In addition Hall effect and sheet resistance measurements were made to determine the number of carriers/ $\text{cm}^2$  and their mobility.

Implantation conditions and isochronal anneal sequences were chosen similar to those used in earlier investigations of Group III and V dopants where it was found that the implanted ions could occupy well defined lattice locations under these conditions.

## 2. EXPERIMENTAL PROCEDURE

Implantations\* of Rb and Cs were made at energies between 5 and 50 keV into 100 to 30,000  $\Omega\text{-cm}$  *p*-type etch-polished, float-zoned Si. Ion doses were between  $5 \cdot 10^{12}$  and  $5 \cdot 10^{14}/\text{cm}^2$ , with substrate temperatures of 350°C and room temperature (R.T.). In this work 9 Cs and 7 Rb implanted samples were evaluated. Subsequent annealing (50°C steps) of the implanted crystals

was performed in a quartz-tube furnace in an atmosphere of dry argon. A 15 min period was used in the isochronal annealing sequences. Samples were divided so that backscattering and Hall effect measurements could be compared for the same samples.

Channeling and backscattering measurements were made at R.T. using a beam of 1 MeV  $^4\text{He}$  ions. The samples were mounted on a goniometer in a target chamber with secondary electron suppression. Analyses were made with the same charge incident upon the target, measured with a current integrator. Energy distributions of backscattered particles were measured with a surface barrier detector. The number of implanted ions can be calculated by comparing the area of the impurity peak with the height of the Si spectrum for random orientation.<sup>(7)</sup> In the aligned case (the incident beam is aligned parallel to the  $\langle 111 \rangle$  or  $\langle 110 \rangle$  crystal axis) the yield from Si is strongly reduced. The orientation dependence of the scattering yield from the impurity atoms can be used to investigate lattice location of the dopants. The aligned spectra (Si) were used to determine the amount of disorder introduced during implantation and subsequent reordering of the lattice during heat treatment.<sup>(8)</sup> The linear energy scale provided by the semiconductor nuclear particle detector may be converted into a depth scale. The system resolution corresponded to 6–8 keV (100–150Å) and was less than the width of the impurity distribution. Thus, the impurity spectrum produced by  $^4\text{He}$  ions backscattered from the implanted impurity atoms is nearly an image of the depth distribution of the implanted ions.

Hall effect and sheet resistivity measurements<sup>(2,9)</sup> were made using the van der Pauw method to determine an effective surface concentration  $N_s$  in carriers/ $\text{cm}^2$  and an effective mobility  $\mu_H$ . The implanted surface is etched to form a mesa by use of photoresist techniques. The necessary electrical isolation between bulk silicon and ion implanted layer was checked during measurements by monitoring the reverse current across the junction (which was small compared to the measurement current). For a further control, the photoresponse of the diode was measured. In all cases the ratio of Hall mobility and conductivity mobility was taken to be 1. Since in ion implanted

\*Implantations were made at the Research Institute for Physics, Stockholm and the Nuclear Research Center, Karlsruhe. In general, no deliberate attempt was made to align the crystal with the incident beam.

layers carrier concentration and carrier mobility are depth dependent, the measured values  $N_s$  and  $\mu_H$  are weighted averages. These factors might result in a 20–30 per cent difference<sup>(2,9)</sup> between the measured value of  $N_s$  and the actual number of carriers per  $\text{cm}^2$ .

### 3. RESULTS

#### A. Backscattering data

Figure 1 shows the impurity peak portion of the energy spectra obtained for  $^4\text{He}$  ions backscattered

impurity spectra. This was true for samples implanted at R.T. as well as at  $350^\circ\text{C}$  substrate temperature, for anneal temperatures up to  $1100^\circ\text{C}$  and a dose range between  $5 \cdot 10^{13}$  and  $5 \cdot 10^{14}/\text{cm}^2$ . From these results we concluded that less than 10 per cent of the implanted Rb and Cs atoms lie within  $0.1\text{--}0.2\text{\AA}$  of either tetrahedral interstitial or substitutional lattice sites. The lattice sites are defined in respect to the underlying lattice. The exact lattice location cannot be specified from this type of measurement when there is no decrease

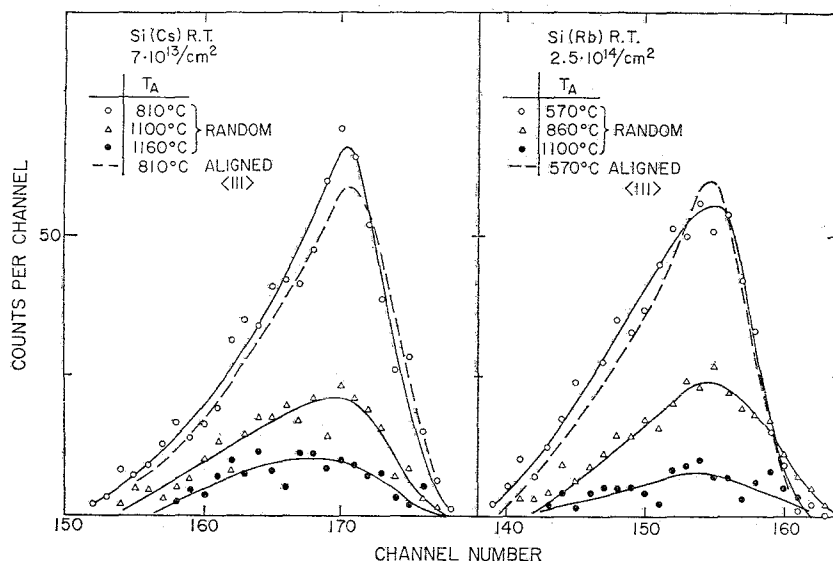


FIG. 1. The energy spectra of MeV  $^4\text{He}$  particles backscattered from Cs and Rb atoms implanted into Si at room temperature. Random impurity spectra for Cs and for Rb are shown for annealing at 810, 1100 and  $1160^\circ\text{C}$  and at 570, 860 and  $1100^\circ\text{C}$ , respectively. The random spectra for 810 and  $570^\circ\text{C}$  coincide with the as-implanted spectra. The aligned  $\langle 111 \rangle$  spectra are given as a dashed line.

from samples implanted with Rb and Cs at R.T. and 50 keV. The impurity peaks for Cs are shown after annealing the samples at 810, 1100, and  $1160^\circ\text{C}$  and for Rb after annealing at 570, 860 and  $1110^\circ\text{C}$ . The impurity peak spectra measured after implantation coincided in height and width with the given spectra at  $910^\circ\text{C}$  for Cs and at  $570^\circ\text{C}$  for Rb, respectively. The dashed line in Fig. 1 indicates the aligned spectra. In almost every case investigated, the total number of counts in the aligned spectra ( $\langle 111 \rangle$  and  $\langle 110 \rangle$ ) was never less than 90 per cent of the total number in the random

in the aligned impurity spectra. It is possible that lattice distortions in the implanted layer might be responsible for the nonregular positions measured.

The values of the full width at half maximum (FWHM) of the impurity peak spectra in all samples implanted at 50 keV were larger than the detector resolution. In these cases, the impurity spectra can be used to determine the impurity distribution, and the average concentration,  $\bar{n}$ , of implanted species can be estimated from the number of atoms/ $\text{cm}^2$  and the FWHM. In Fig. 1, at the lowest anneal temperatures, the FWHM of

36 keV were equivalent to about  $540\text{\AA}$  and the average concentrations were  $4.5 \times 10^{19}/\text{cm}^3$  for Rb and  $1.3 \times 10^{19}/\text{cm}^3$  for Cs.

During anneal sequences at elevated temperatures (Fig. 1), the total number of counts in the random spectra decreased and there was no apparent motion of atoms deeper into the crystal. This indicates that outdiffusion was taking place. Diffusion toward the surface seems to be an effect which is common in ion implanted layers.<sup>(10,11)</sup> For Rb and Cs implanted samples outdiffusion occurs at temperatures above that where the lattice disorder anneals. In R.T. implanted Rb samples outdiffusion of about 60 per cent of the Rb ions was observed in the temperature range between 650 and 750°C; in 350°C implantations about a 20 per cent decrease in the impurity peak in the same temperature range. For both implantation conditions further outdiffusion was noted for anneal temperatures  $\geq 900^\circ\text{C}$ . In Cs samples outdiffusion was observed at  $T_A \geq 900^\circ\text{C}$  for R.T. implantation as well as for implantations at 350°C substrate temperature. For both species no apparent peak shift towards the surface, nor pile up near the silicon-oxide interface was found (as was observed for Cd and Se implantations<sup>(11)</sup>).

### B. Electrical behavior

(a) *Implantations into R.T. Si substrates.* Figure 2 shows the number of carriers/cm<sup>2</sup>,  $N_s$ , and their mobility vs. anneal temperature for two Rb samples implanted at R.T. with  $5 \cdot 10^{13}$  and  $2.5 \cdot 10^{14}$  ions/cm<sup>2</sup>. The maximum  $N_s$  values,  $N_{s(\text{max})}$ , are found between 700 and 750°C and correspond to about 7 per cent of the implanted number of ions/cm<sup>2</sup>,  $N_D$ , for the high dose and to about 12 per cent for the low dose sample. From the values of  $N_s$  (which do not show a big increase with increasing  $N_D$ ) together with the measured FWHM, we estimate that the maximum value of the average carrier concentration is about  $5 \cdot 10^{18}/\text{cm}^3$  at 750°C. The temperature range where the maximum values for  $N_s$  are found, lies well above the temperature range where the lattice reorders. This is in contrast to Sb and Ga implanted (R.T.) layers, for example, in which the maximum values of  $N_s$  were noted<sup>(12)</sup> in the region where the amorphous layer reordered ( $\sim 550^\circ\text{C}$ ). The decrease in the Hall mobility  $\mu_H$  coincides with the increase in  $N_s$ . The  $\mu_H$  values measured in the region of

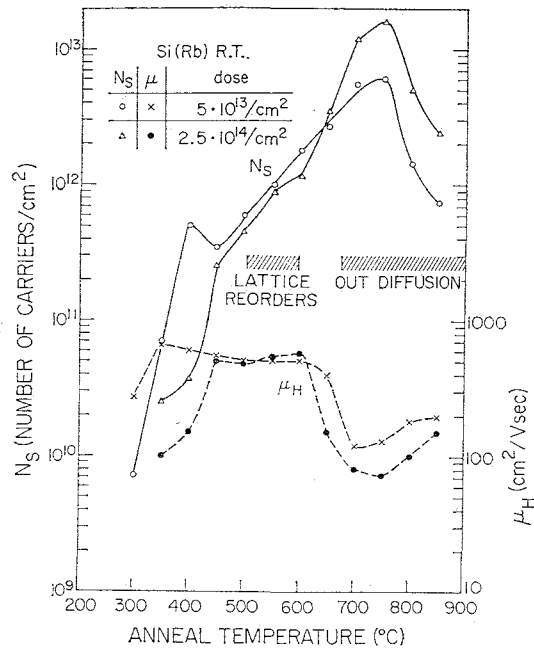


FIG. 2. Effective number of carriers/cm<sup>2</sup>,  $N_s$ , and Hall mobility,  $\mu_H$ , vs. isochronal anneal temperature for Rb ( $5 \cdot 10^{13}$  and  $2.5 \cdot 10^{14}$  Rb<sup>+</sup>/cm<sup>2</sup>) in Si at R.T.

$N_{s(\text{max})}$  are comparable or slightly lower than the  $\mu_H$  values that one would calculate from the carrier concentration.

The results for Cs layers implanted at R.T. are given in Fig. 3. The shapes of the curves are nearly identical to that for Rb with the exception that  $N_{s(\text{max})}$  is about a factor of 5 lower. The value of  $N_{s(\text{max})}$  is about 1-4 per cent of  $N_D$  for doses between  $5 \cdot 10^{13}$  to  $5 \cdot 10^{14}$  ions/cm<sup>2</sup>. From the measured FWHM, it is found that the maximum average carrier concentration is about  $0.5$  to  $1 \cdot 10^{18}/\text{cm}^3$ . The decrease in  $N_s$  occurs at the same temperatures where the drop of  $N_s$  for Rb implants was noticed. Investigations with lower dose Cs implanted at R.T. with 5 keV exhibited the same shape as that for the 50 keV implants. In this case the value of  $N_{s(\text{max})}$  was about 4 per cent of the implanted dose. The decrease in  $N_s$  was found to occur in the same anneal temperature region as that for 50 keV implants.

The Hall mobility in Fig. 2 for  $T_A$  about 700°C is slightly higher than that for Rb, but it is appreciably lower than one should expect from calculated values for that carrier concentration.

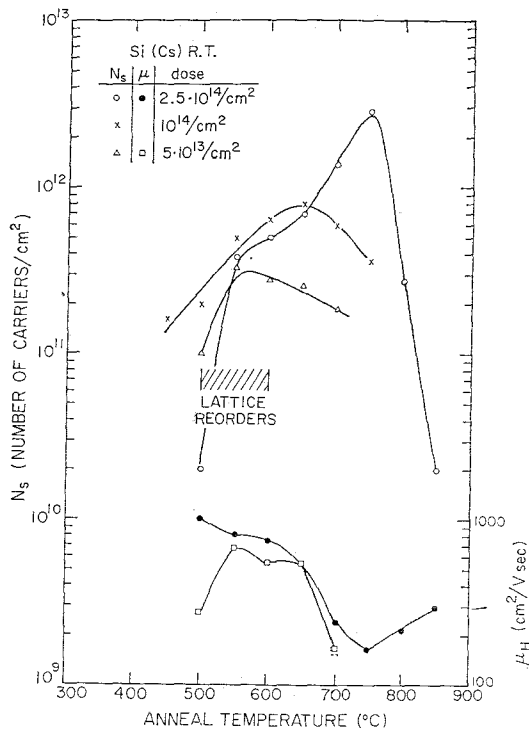


FIG. 3. Effective number of carriers/cm<sup>2</sup>,  $N_s$ , and Hall mobility,  $\mu_H$ , vs. isochronal anneal temperature for Cs implanted in Si at R.T. with doses of  $5 \cdot 10^{13}/\text{cm}^2$ ,  $10^{14}/\text{cm}^2$  and  $2.5 \cdot 10^{14}/\text{cm}^2$ .

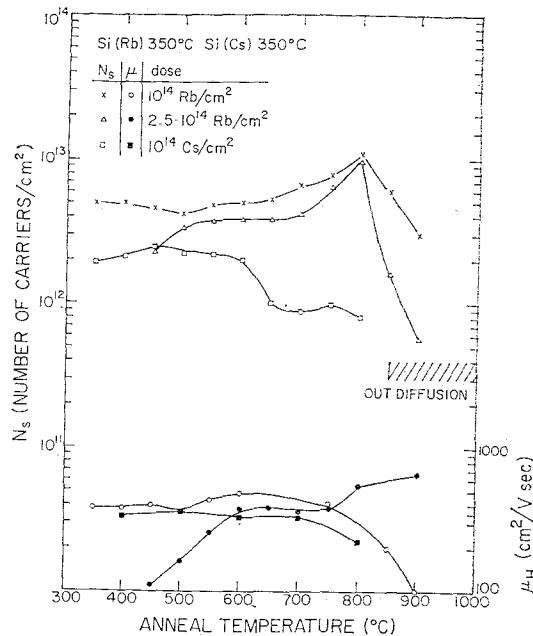


FIG. 4. Effective number of carriers/cm<sup>2</sup>,  $N_s$ , and Hall mobility,  $\mu_H$ , vs. isochronal anneal temperature for Rb ( $10^{14}$  Rb<sup>+</sup>/cm<sup>2</sup>,  $2.5 \cdot 10^{14}$  Rb<sup>+</sup>/cm<sup>2</sup>) and Cs ( $10^{14}$  Cs<sup>+</sup>/cm<sup>2</sup>) implanted in Si at 350°C.

(b) *Implantations into Si substrate at 350°C.* The results of the Hall measurements presented in Fig. 4 show that  $N_{s(\text{max})}$  for Rb occurs roughly in the same temperature region as that for R.T. implanted samples. This was not found in Hall measurements on Group III and V elements<sup>(2)</sup> where it was noted that for hot implants, the maximum electrical activity is achieved at higher anneal temperatures than for R.T. implants. For Rb, the maximum value of  $\bar{n}$  is about  $2 \cdot 10^{18}/\text{cm}^3$  at 800°C; this is a slightly lower value than that obtained for R.T. implanted layers. For  $T_A \lesssim 650^\circ\text{C}$ ,  $N_s$  is nearly independent of the annealing temperature. The Hall mobility values over the total anneal temperature range is nearly constant between 300 and 400 cm<sup>2</sup>/V sec. This corresponds to a calculated carrier concentration of  $10^{18}/\text{cm}^3$ , which agrees with measured concentration. For 350°C Cs implantations the values of  $N_s$  did not vary strongly with anneal tempera-

ture. The values of  $N_s$  were about 1 per cent of the implanted dose.

#### 4. DISCUSSION AND SUMMARY

The behavior of implanted Rb and Cs in Si is different in almost every respect compared with the behavior of Group II, III, V and VI implants.

##### (a) *Lattice locations*

In these measurements neither Rb nor Cs were found to be on substitutional or tetrahedral interstitial lattice sites to levels greater than 10 per cent. This does not preclude the possibility of other regular lattice sites. The absence of a defined lattice position cannot be attributed to thermal solubility conditions. Under similar implantation and anneal conditions<sup>(7,8)</sup> Group II, III, V and VI implanted species can occupy regular lattice sites, irrespective of their solubility values. It is possible that the lattice is distorted due to defects introduced during implantation, however, the disorder annealed in a fashion similar to that

of other implanted species. Nevertheless, distortions or defects below the detectable limit might be present. We suggest that, because of the large size of the ionic radii, the species are displaced from regular sites.

#### (b) Outdiffusion

Outdiffusion effects were observed which seem to influence the electrical behavior. However, a direct connection between the decrease of carriers/cm<sup>2</sup> and a decrease of the total number of implanted ions could not be established. For Cs implanted samples, the decrease in  $N_s$  occurred about 200°C below that for outdiffusion. In Rb samples implanted at R.T. outdiffusion starts about 70°C before the decrease of  $N_s$  is observed, whereas in hot implants the decrease of  $N_s$  seems to be connected with outdiffusion. Therefore a precipitation process connected with the decrease of  $N_s$  cannot be excluded. A case illustrating precipitation, for example, was found<sup>(11)</sup> in hot Zn implants in Si where the decrease in  $N_s$  was connected with the decrease of the tetrahedral interstitial component between 500 and 600°C whereas outdiffusion occurred between 700 and 800°C. The influence of diffusion on electrical properties was found,<sup>(11)</sup> for example, in Se implanted silicon in which a decrease in  $N_s$  could be connected with enhanced diffusion towards the surface and precipitation at the silicon-oxide interface.

#### (c) Electrical behavior

The maximum carrier concentration measured was about  $5 \cdot 10^{18}/\text{cm}^3$  for Rb and about  $10^{18}/\text{cm}^3$  for Cs. Both values seem to be an upper limit under these implantation conditions. These values are somewhat lower than reported in earlier measurements.<sup>(5)</sup> Nevertheless they are comparable to or higher than those obtained for Te, Cd, Zn, In and Tl implants and about 1–2 orders of magnitude lower than that of other Group III and V elements.<sup>(2)</sup> For R.T. Rb implants the increase in  $N_s$  is not connected with the reordering of the amorphous layer as it is usually found for Group III

and V implants.<sup>(2,12)</sup>  $N_{s(\text{max})}$  for Rb was obtained in the temperature range between 700 and 800°C for R.T. as well as for hot implant conditions; this again is in contrast to Group III and V implants where  $N_{s(\text{max})}$  for R.T. implanted samples is generally obtained between 500 and 600°C, whereas for hot implants the maximum electrical activity is found<sup>(2,12)</sup> at 700–800°C. For the Rb and Cs samples investigated the values of  $N_s$  were comparable to the lower limit established in channeling effect measurements. Consequently, it is not possible to decide whether the electrical activity arises from implanted species on non-regular lattice sites or on tetrahedral interstitial (or substitutional) sites.

*Acknowledgements*—The authors acknowledge with pleasure discussions with J. GYULAI, N. G. E. JOHANSSON, and S. T. PICRAUX about the behavior of implanted species.

#### REFERENCES

1. L. ERIKSSON, J. A. DAVIES, N. G. E. JOHANSSON and J. W. MAYER, *J. appl. Phys.* **40**, 842 (1969).
2. R. BARON, G. A. SHIFRIN, O. J. MARSH and J. W. MAYER, *J. appl. Phys.* **40**, 3702 (1969).
3. S. T. PICRAUX, N. G. E. JOHANSSON and J. W. MAYER, *Semiconductor Silicon* (Ed. R. R. HABERECHE and E. L. KERN) p. 422 Electrochem. Soc. Inc., New York (1969).
4. J. O. McCALDIN and A. E. WIDMER, *J. Phys. Chem. Solids* **24**, 1073 (1963).
5. J. O. McCALDIN, *Progress in Solid State Chem.* (Ed. H. REISS) Vol. 2, p. 9. Pergamon Press, Oxford (1965).
6. D. B. MEDVED, J. PEREL, H. L. DALEY and G. P. ROLIK, *Nucl. Instrum. Meth.* **38**, 175 (1965).
7. J. A. DAVIES, J. DENHARTOG, L. ERIKSSON and J. W. MAYER, *Can. J. Phys.* **45**, 4073 (1967).
8. J. W. MAYER, L. ERIKSSON, S. T. PICRAUX and J. A. DAVIES, *Can. J. Phys.* **46**, 663 (1968).
9. N. G. E. JOHANSSON, J. W. MAYER and O. J. MARSH, *Solid-St. Electron.* **13**, 317 (1970).
10. C. JECH and R. KELLY, *J. Phys. Chem. Solids* **30**, 465 (1969).
11. O. MEYER and J. W. MAYER, *J. appl. Phys.* (to be published Aug. 1970).
12. N. G. E. JOHANSSON and J. W. MAYER, *Solid-St. Electron.* **13**, 123 (1970).

## COMMUNICATION

## ENHANCED OXIDATION ON ION-IMPLANTED SILICON†

O. MEYER‡ AND J. W. MAYER

California Institute of Technology, Pasadena, California 91109, U.S.A.

We have found that enhanced oxidation occurs on ion-implanted silicon samples during anneal sequences from 600 to 1100 °C. The amount of oxidation depends on the implanted species and in some cases, the ion dose. Backscattering and channeling effect measurements were used to determine the number of oxygen and displaced silicon atoms.<sup>(1,2)</sup>

Implantations were made at room temperature and 50 keV into 100  $\Omega$ -cm *n*- and *p*-type float-zoned silicon. Doses were between  $8 \times 10^{13}$  and  $1 \times 10^{15}$  ions/cm<sup>2</sup> for Rb, Cs, Cd, I, Se, and Sb. Subsequent annealing of the implanted crystals in 50° steps was performed in a quartz-tube furnace in an atmosphere of dry argon for 15 minute isochronal anneal sequences. In some cases where differences of oxidation rate were observed, samples were annealed at the same time and adjacent to each other. Non-implanted samples were annealed under the same conditions for comparison.

Analyses of the implanted samples were made at room temperature with 1 MeV <sup>4</sup>He ions. Energy distributions of the backscattered particles were measured with a surface barrier detector. The energy resolution of the detecting system was about 6 to 8 keV for the beam energy and experimental geometry used. The samples were mounted on a goniometer in the target chamber with secondary electron suppression. The analyses were made using the same integrated beam current on the target. Figure 1 shows random and aligned spectra for different implanted samples after anneal at 1100 °C. The spectra for non-implanted samples are given for 850 °C and 1100 °C. The peaks at lower channel numbers are due to <sup>4</sup>He ions backscattered from oxygen atoms located in the oxide layer on the surface. The peaks in the aligned spectra at higher channel numbers are due to scattering from Si atoms in the oxide layer and displaced atoms (including the first layer) in the surface

† Work supported in part by NSF GP-9114 and A. F. Cambridge Research Laboratories.

‡ Permanent Address: Inst. f. Angew. Kernphysik, Kernforschungszentrum, Karlsruhe.

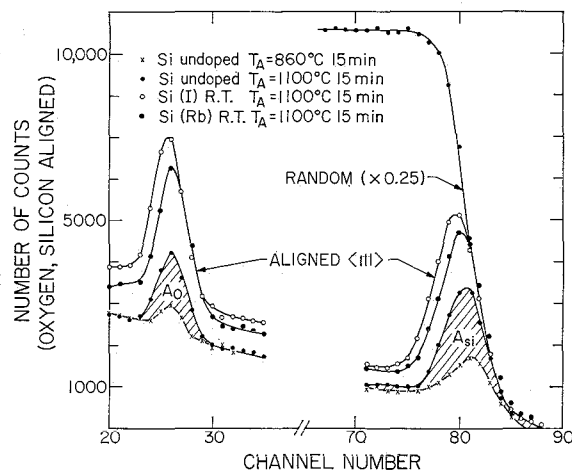


FIG. 1. The energy spectra of MeV <sup>4</sup>He particles backscattered from silicon for random and aligned orientation. Spectra are shown for an undoped silicon sample annealed at 850 and 1100 °C and for 50 keV room temperature Rb and I implantation after anneal at 1100 °C. The peaks at lower channel numbers correspond to scattering from oxygen atoms and that at higher energy from silicon atoms located at the surface.

region. The shaded areas  $A_O$ ,  $A_{Si}$  represents the increase in the number of oxygen and silicon atoms during the anneal of the non-implanted sample. The ratio of the total numbers is given by  $(A_O/A_{Si}) \times (\sigma_{Si}/\sigma_O)$  where  $\sigma$  is the backscattering cross-section in the laboratory system. The number of Si ( $N_{Si}$ ) and O ( $N_O$ ) atoms/cm<sup>2</sup> can be obtained<sup>(1)</sup> by comparison of peak area with the height,  $R_{Si}$ , of the random spectrum in one channel near the surface:

$$N_{Si,O} = n_{Si,O} \sigma_{Si,O} A_{Si,O} \delta E (R_{Si} \sigma_{Si,O} [S_{Si}])^{-1}$$

where  $n_{Si}$  is  $5 \times 10^{22}$  Si/cm<sup>3</sup>,  $\delta E$  is the calibrated energy per channel, and  $[S_{Si}]$  is the backscattering energy loss parameter.<sup>(3)</sup> For the experimental arrangement and the beam energy used  $[S_{Si}] = 51$  eV/Å.

From the peak areas in the spectrum obtained for undoped Si after anneal for 15 min. at 850 °C, the

ratio  $N_O/N_{Si}$  is approximately unity similar to that, usually found for non-implanted unannealed Si samples.<sup>(1)</sup> The ratio of  $N_O/N_{Si}$  in the shaded areas however, is found to be 2; this shows that a stoichiometric oxide is growing during the heat treatment. The far larger peak areas for I and Rb implanted layers, annealed at the same time under the same conditions as the undoped sample clearly show the enhanced oxidation. Enhanced oxidation was not found, for example, on Cd, and Sb implanted samples.

The increase of the number of O atoms/cm<sup>2</sup> with increasing anneal temperature for an undoped sample and samples implanted with Rb, I, Cs, and Se is given in Figure 2. Two different oxidation mechanisms were found: the steep rise for the I implanted sample for temperatures >900°C and for the Se implanted sample for temperatures >1000°C, were found to be stoichiometric and can be described by an enhanced growth of thermal oxide, whereas the Rb and Cs implanted samples were found to be oxygen rich with  $N_O/N_{Si} \approx 3$  over the total temperature range observed. The numbers of Rb and Cs atoms/cm<sup>2</sup> are approxi-

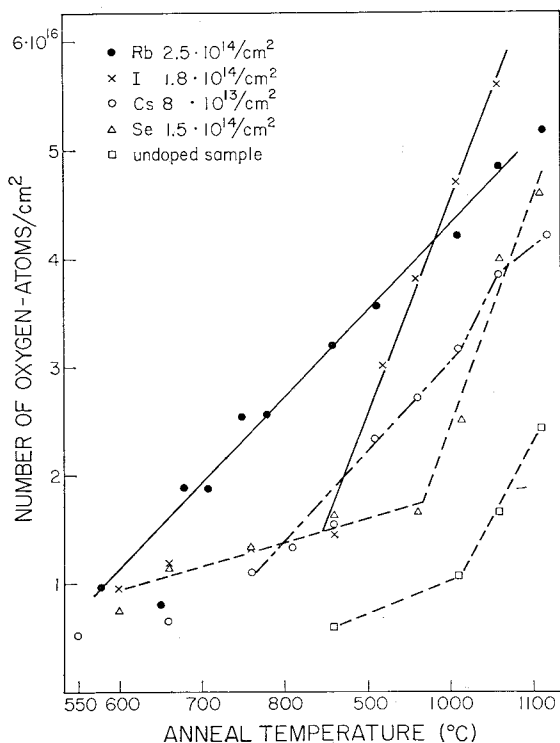


FIG. 2. Number of oxygen atoms versus anneal temperature for different implanted species.

mately two orders of magnitude less than the number of O atoms/cm<sup>2</sup>.

Enhanced oxidation was found also on samples, where Rb was implanted at 350° substrate temperature. Under these implantation conditions, the disorder is greatly reduced. Thus the high lattice disorder generally found in room temperature implants and which anneals in the temperature range between 500° and 600°C is not the dominant influence on the enhanced oxidation in this case. Rb as well as Cs outdiffusion was observed in the temperature ranges between 500° and 1100°C for Rb and between 900° and 1150°C for Cs. Thus the steady flow of Rb as well as Cs ions through the surface layer during the temperature treatment may have enhanced the oxidation, even if  $Rb_xO_y$  and  $Cs_xO_y$  are not stable for temperatures greater than 650°C.

For Rb and Cs samples implanted at R.T., 5 keV with doses of about  $10^{15}$  ions/cm<sup>2</sup> relative higher numbers of oxygen atoms/cm<sup>2</sup> (about 50 per cent) were observed at comparable temperatures. Thus the enhanced oxidation for Rb and Cs implanted samples seems to be dose dependent.

The full width at half maximum (FWHM) of the disorder peak stays constant within the limits of statistical error during the heat treatment, whereas the FWHM for the oxide peak slowly increases with increasing temperature. The ratio  $FWHM_{Si}/FWHM_O$  decreases with increasing temperature, in case of I at the highest temperature measured it approaches the value of 1.25, which is usually found in thick oxide layers.<sup>(3)</sup>

The presence of enhanced oxidation and its species dependence may have an influence on analyses of other aspects of implantation phenomena. The surface peak usually used to study lattice disorder for low energy ( $\leq 50$  keV) implants might be influenced by the enhanced growth of the oxide layers. Enhanced oxidation could also influence outdiffusion and gas release studies if the transport through an oxide layer was the rate limiting process.

#### REFERENCES

1. J. A. Davies, J. Denhartog, L. Eriksson, and J. W. Mayer, *Can. J. of Phys.*, **45**, 4703 (1967).
2. L. Eriksson, J. A. Davies, N. G. E. Johansson, and J. W. Mayer, *J. Appl. Phys.*, **40**, 842 (1969).
3. O. Meyer, J. Gyulai, J. W. Mayer, to be published (*Surface Science*).

Received 3 February 1970

## ENHANCED OUTDIFFUSION IN ION IMPLANTED SILICON ‡

O. MEYER\* and J. W. MAYER  
*California Institute of Technology*

Received 28 January 1970

The distribution of ions implanted in Si at 50 to 400 keV have been found to shift preferentially towards the surface during thermal anneal sequences. This suggests that outdiffusion studies as gas-release may not represent bulk diffusion properties in crystals.

We have investigated thermal diffusion of ion implanted species in Si by use of backscattering and channeling effect measurements of 1 MeV  $^4\text{He}$  ions. The purpose of this work was to study the factors which influence outdiffusion of non-gaseous species implanted in Si. Previous work on outdiffusion has primarily dealt with release of radioactive inert gases to determine diffusion coefficients and activation enthalpies [1,2]. In previous studies [3] of lattice location of the group III and V elements, significant outdiffusion was not observed at temperatures up to 900°C.

Si samples used in this work were 100 to 30 000 $\Omega$ -cm n and p-type float-zone material. Implantations were made at 50 keV and room temperature and 350°C substrate temperature of Group I (Rb, Cs), Group II (Zn, Cd, Hg, Cu) and Group VI (Se, Te) elements and at 400 keV at room temperature for Sb and In. No deliberate attempt was made to align the ion beam direction with crystal axes or planes. Ion doses were between  $5 \times 10^{13} \text{ cm}^{-2}$  and  $2 \times 10^{15} \text{ cm}^{-2}$ . Subsequent annealing was performed in a quartz-tube furnace in an atmosphere of dry argon with isothermal and isochronal (15 min.) annealing sequences. Analyses of the implanted samples was made with 1 MeV  $^4\text{He}$  ions using backscattering techniques to determine the total number of the implanted ions and their depth distribution and channeling effect measurements to determine lattice disorder and the lattice location of implanted species [3]. For the beam energy and the experimental geometry used the energy resolution of the surface-barrier detector system was 6 to

8 keV corresponding to a depth resolution of 100 to 150 Å (less than the width of the distribution of the implanted ions in all cases).

Fig. 1 shows the energy distribution of  $^4\text{He}$  ions backscattered from Sb implanted at 400 keV (the dashed line shows the initial distribution). In the isothermal anneal sequences it can be seen that the distributions at lower channel numbers (i.e. at deeper depth in the crystal) are relatively unchanged. However, there is a decrease observed in the height of the distribution and also a broadening of the distribution towards the surface. The observed asymmetrical distribution is indicative of a non-constant diffusion coefficient throughout the implanted layer. The solid lines are the calculated [4] distributions with a value of  $D = 10^{-16} \text{ cm}^2/\text{sec}$  (the normal value for Sb at 900°C) for the deeper flank of the profile, whereas a higher diffusion coefficient  $D = 3.3 \times 10^{-15} \text{ cm}^2/\text{sec}$  described peak decrease as well as the region from peak to the surface after different isothermal anneal times. The integrated number of counts under the impurity peak was constant throughout the isothermal anneal sequence at 900°C. At the surface, the growth of a peak in the impurity distribution indicated that Sb ions have diffused to the surface and become trapped there and the aligned spectrum indicated, that these atoms were not on substitutional lattice sites.

Outdiffusion rate-limiting processes at the surface were also observed for Cd and Se implanted samples. Room temperature distributions of both species implanted at 50 keV had a peaked shape with a tail to deeper depth. With increasing temperature in an isochronal treatment a peak shift towards the surface was observed ( $T_A \geq 600^\circ \text{C}$  for Se,  $600^\circ \leq T_A \leq 900^\circ \text{C}$  for Cd), the width decreased more than a factor of two

‡ Work supported in part by NSF 69-9114 and A. F. Cambridge Research Labs.

\* Permanent address: Institut für Angewandte Kernphysik, Kernforschungszentrum, Karlsruhe.

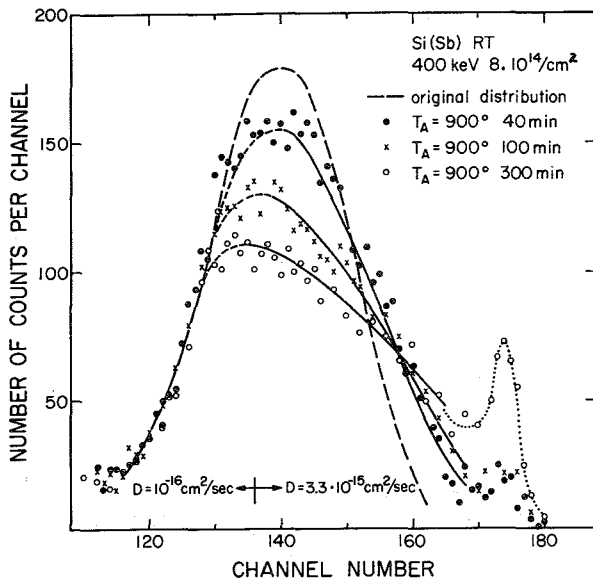


Fig. 1. Random energy spectra of MeV  $^4\text{He}$  ions back-scattered from Sb atoms implanted in Si at 400 keV. 10 channels correspond to a depth of 560 Å.

whereas the total number of atoms stayed constant. Further increase of temperature ( $T_A \geq 900^\circ\text{C}$ ) lead to a sudden decrease of the total number of Cd atoms (outdiffusion). A peak shift and a decrease of FWHM was not observed during outdiffusion of Cs, Rb, Zn, Hg and I. However, in no case was there broadening of the distribution into the sample.

The anneal of lattice disorder can also have a large influence on the outdiffusion of implanted species. It was observed that for room temperature implanted Zn and Cd atoms the decrease in the number of atoms coincides closely with the reordering of the amorphous layer ( $470^\circ \leq T_A \leq 600^\circ\text{C}$ ). For implantations at  $350^\circ\text{C}$ , however, the decrease in both the total number of Zn and Cd atoms occurred at significantly higher temperature ( $T_A \geq 650^\circ\text{C}$  for Zn,  $T_A \geq 900^\circ\text{C}$  for Cd). Here the tetrahedral interstitial component decreased (precipitation) at temperatures below outdiffusion ( $500^\circ \leq T_A \leq 650^\circ\text{C}$  for Zn and  $600^\circ \leq T_A \leq 750^\circ$  for Cd).

These results indicate that extreme care must be exercised when determining diffusion coefficients or activation enthalpies from either gas release measurements or just observation in the decrease of the total number of implanted atoms. It is necessary to look at the distribution and lattice location of implanted atoms to determine that there are no factors influencing outdiffusion.

#### References

1. C. Jech and R. Kelly, *J. Phys. Chem. Solids* 30 (1969) 46
2. R. Kelly and H. J. Matzke, *J. Nucl. Mat.* 20 (1966) 171.
3. L. Eriksson, J. A. Davies, N. G. E. Johansson and J. W. Mayer, *J. Appl. Phys.* 40 (1969) 842.
4. T. E. Seidel and A. U. MacRae, *Trans. AIME* 245 (1969) 491.

\* \* \* \* \*

## Enhanced Diffusion and Out-Diffusion in Ion-Implanted Silicon\*

O. MEYER† AND J. W. MAYER

*California Institute of Technology, Pasadena, California 91109*

(Received 2 February 1970)

Backscattering and channeling-effect measurements were used to determine the lattice disorder and distribution, lattice location, and diffusion of species (Rb, Cs, Zn, Cd, Hg, Se, I, and Sb) implanted in Si. During anneal sequences we observed (1) enhanced diffusion towards the surface (Sb, Se, and Cd), (2) retardation or precipitation at the surface (Sb, Se, and Cd), and (3) a connection between out-diffusion and reordering of the amorphous layer (Zn, Cd, Hg, and I). The data also suggest that release of atoms from trapping (precipitation) sites in the implanted layer can be the rate-limiting process in some cases. These results indicate that out-diffusion studies such as gas release, may not represent bulk diffusion properties in crystals.

### I. INTRODUCTION

In this paper we describe the depth distribution, lattice location, and diffusion of ion-implanted species in Si as a function of anneal temperature. Particular emphasis is placed on factors which influence out-diffusion of the implanted atoms. Backscattering of million electron-volt He ions was used to determine the depth distribution and total number of implanted atoms. Channeling effect measurements<sup>1</sup> were used to study lattice disorder<sup>2</sup> and the lattice location<sup>3</sup> of the implanted species. Earlier, backscattering techniques had been used to study the diffusion of Au in Cu.<sup>4</sup>

In lattice location studies and Hall effect measurements of group II and VI elements implanted in silicon,<sup>5</sup> a strong decrease of the total number of atoms or the total number of charge carriers was found during anneal sequences. Such effects are of course of some practical importance when considering ion implantation as a means of doping semiconductors. Further, motions of atoms from substitutional lattice sites to interstitial positions as well as motions from those regular lattice sites to nonregular lattice positions have been observed at temperatures well below those at which normal diffusion becomes significant.<sup>3</sup> The purpose of this paper was to study the factors which may influence the out-diffusion process, such as disorder, radiation enhanced diffusion, precipitation in the bulk or at the surface, and surface permeability. The reordering of the amorphous layer for example was found to influence the out-diffusion (release) of inert gases implanted in silicon and germanium.<sup>6</sup> In fact, inert gas release has been used as a probe to study annealing of radiation damage introduced during implantation.<sup>6</sup> In other work, the kinetics of gas release from implanted samples has been analyzed to determine diffusion rates.<sup>7,8,9</sup> Out-diffusion is a well-known phenomenon in semiconductor technology and has been used, for example, to produce special impurity distributions useful in device fabrication.<sup>10,11</sup>

Our measurements deal mostly with group I and II ions, where out-diffusion has a strong effect at relatively low anneal temperatures. For normal group III and V elements out-diffusion is usually not observed at temperatures below 850°C. In this work, we studied primarily two well-defined initial conditions: (a) room-

temperature-implanted samples, where an amorphous layer is formed, and (b) elevated-temperature implants (350°C) where disorder is much reduced and ions can occupy regular lattice sites.

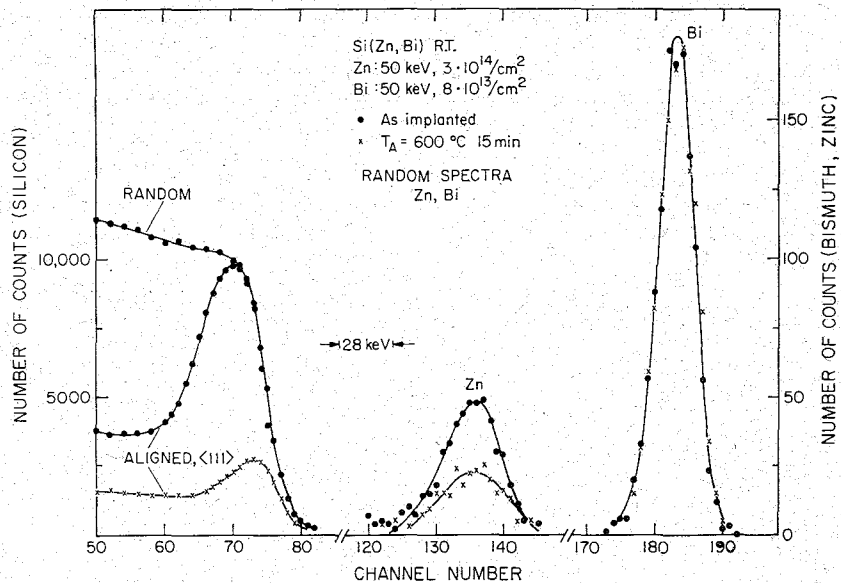
### II. EXPERIMENTAL

The silicon samples used in these experiments were 100–30 000  $\Omega$  cm, *n*- and *p*-type float-zone material. Implantations were carried out at ion energies between 5 and 400 keV using dose rates between  $10^{11}$  and  $10^{12}$  ions  $\text{cm}^{-2} \text{sec}^{-1}$ . (Implantations were made at the Research Institute for Physics, Stockholm, Aarhus University, Aarhus, and Nuclear Research Center, Karlsruhe.) No deliberate attempt was made to orient the crystal with the incident beam. Subsequent annealing of the implanted crystals was performed in a quartz-tube furnace in an atmosphere of dry argon in isothermal and isochronal annealing sequences. A 15-min period was used in the isochronal heat treatments which were carried out in 50°C steps.

Analyses of the implanted samples were made at room temperature using wide-angle elastic scattering, (backscattering) and channeling of 1-MeV  $^4\text{He}$  ions. Energy distributions of backscattered particles were measured with a surface barrier detector. The ultimate depth resolution was set by the energy resolution of the detecting system; it was about 10–14 keV for the beam energy and experimental geometry used. This is equivalent to a depth of 180–240 Å. The samples were mounted on a goniometer in the target chamber with secondary electron suppression. The charge incident upon the target during analysis was measured with a current integrator. For cryogenic detector operation, energy resolution was about 6–8 keV, corresponding to a depth scale of 100–150 Å.

Energy spectra of  $^4\text{He}$  ions, backscattered from a silicon sample implanted with Zn and Bi both at 50 keV are shown in Fig. 1. As long as the masses of the implanted atoms are significantly heavier than that of Si (as those shown for example in Fig. 1) the  $^4\text{He}$  ions scattered show well-resolved peaks. The difference in the areas underneath the Bi and Zn peak in Fig. 1 is due to the  $Z^2$  dependence of the Rutherford scattering cross section. The number of implanted ions can be

FIG. 1. Random and  $\langle 111 \rangle$  backscattering energy spectra using 1-MeV  $^4\text{He}$  ions for a 50-keV mixed RT Zn and Bi implant ( $3 \times 10^{14}$  Zn/cm $^2$ ,  $8 \times 10^{13}$  Bi/cm $^2$ ) in silicon. Note the decrease in Si disorder (aligned spectra) and random Zn spectra during anneal. Ten channels correspond to 560 Å; the energy to channel number conversion gain can be found from the 28-keV energy interval.

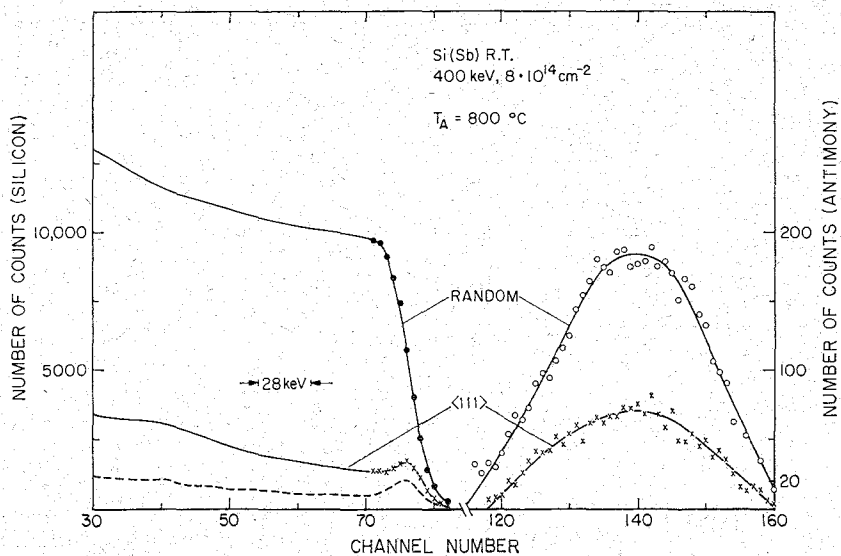


calculated by comparing the area of the impurity peak with the height of the Si spectrum for random orientation. In Fig. 1, aligned and random spectra for the yield of  $^4\text{He}$  ions, backscattered from the silicon lattice are shown. In the random case the spectrum is nearly rectangular, whereas in the aligned case (the incident beam is aligned parallel to the  $\langle 111 \rangle$  crystal axis) the observed scattering yield is reduced. The area of the surface peak represents the amount of disorder, i.e., the number of Si atoms displaced off-lattice sites by  $\geq 0.1$ – $0.2$  Å. The drop of the surface peak as a function of anneal temperature (shown for 600°C, 15 min in Fig. 1) indicates the reordering of the lattice. The decrease of disorder during this anneal treatment is accompanied by a decrease of the area underneath the Zn peak (out-diffusion of Zn atoms), whereas the Bi

peak is not affected. It is important to note here that only from the observation of the decrease in both the surface peak (aligned spectra) and the impurity peak (random spectra) a clear picture can be obtained in how far those processes are connected. This is even more important since it was observed that the temperature range where the reordering of the lattice occurs can easily be shifted by about 100°C in isochronal anneal sequences depending on implanted dose, ion species, implantation energy, and possibly other factors.<sup>2,5</sup>

Fig. 2 shows the  $^4\text{He}$  spectra obtained by backscattering from a 400-keV Sb-implanted silicon sample after the sample was annealed for 15 min at 800°C. Because of the high-implantation energy and hence deeper implantation depths in the crystal, the peak maximum is shifted to lower channel numbers; the broad width re-

FIG. 2. Random and  $\langle 111 \rangle$  backscattering energy spectra using 1-MeV  $^4\text{He}$  ions for a 400-keV RT Sb implantation after anneal at 800°C for 15 min. The lower dashed line is the aligned Si spectrum after anneal at 900°C for 300 min (this spectrum corresponds closely to that of a nonimplanted Si sample).



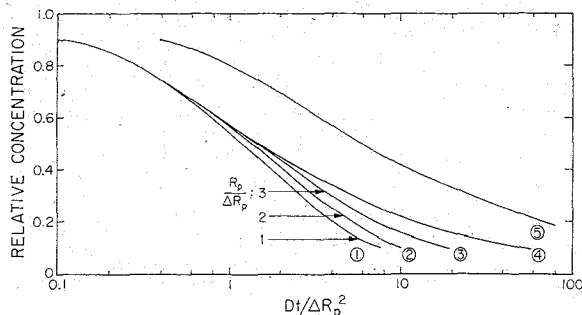


FIG. 3. The relative concentration of implanted atoms as a function of  $Dt/\Delta R_p^2$ . Curves 1-4 represent the relative concentration (number/cm<sup>2</sup> over FWHM) determined for curve 4 from Eq. (2) (no surface sink) and for curves 1-3 for different  $R_p/\Delta R_p$  values from Eq. (4). Curve 5 represents the relative total number of implanted atoms from a peaked distribution with an exponential tail (taken from Matzke<sup>8</sup> with  $R_m = 1.24 R_p$  and  $R_p = 2\Delta R_p$ ).

fects the corresponding high range straggling. For comparison the aligned spectrum is included, it shows that about 70% of the antimony atoms are on regular lattice sites. The decrease in the scattering yield from the silicon lattice indicates, that still an appreciable amount of disorder is left over the total range of implanted Sb. After anneal at 900°C for 300 min (dashed line) the spectrum is similar to that of an undoped sample.

The linear response of semiconductor nuclear particle detectors provides a fixed energy per channel in the multichannel analyzer. The energy scale in Figs. 1 and 2 may be converted into a depth scale from knowledge of the specific energy losses.<sup>1</sup> For a fixed beam energy and experimental geometry the energy loss depends somewhat on the fractional amount of energy after scattering, so the depth scale is different for <sup>4</sup>He ions backscattered from Si atoms or heavier mass atoms. In our experimental setup this parameter varies between 52 and 62 eV/Å; for the impurity peak spectra in Figs. 1 and 2, 10 channels correspond to about 560 Å. The corresponding system resolution lies between 180 and 240 Å. This is small compared to the observed full width at half-maximum (FWHM) for Sb (Fig. 2 about 1500 Å) and Zn (Fig. 1 about 560 Å); and less than the FWHM of the Bi peak. Thus, in most cases, the impurity spectrum produced by <sup>4</sup>He ions backscattered from the implanted impurity atoms, is a direct image of the depth distribution of the implanted ions. By observing changes in the shape of the impurity peak as a function of temperature, for example, it is possible to measure diffusion constants. In other cases diffusion constants can be determined from the decrease in the integral number of impurity atoms in a manner analogous to that used in gas-release studies.

### III. ANALYSIS

For nonchanneled implantation at energies of about 400 keV the peak shape in Fig. 2 is nearly symmetric about the peak maximum and reflects a symmetric depth distribution of the implanted ions. This is in

agreement with other measurements and with theory. In good approximation, this distribution can be described by the equation

$$n(x) = [N_D / (2\pi\Delta R_p^2)^{1/2}] \exp[-(x - R_p)^2 / 2\Delta R_p^2], \quad (1)$$

where  $n$  is the concentration of the implanted ions and  $x$  is the distance from the surface.  $R_p$  is the mean projected range and  $\Delta R_p$  a standard deviation from this mean. For a shape approximately Gaussian,  $R_p$  almost coincides with the position of the peak maximum, whereas  $2.35 \Delta R_p$  is equal to the FWHM.  $N_D$  is the total number of implanted ions per cm<sup>2</sup>. At lower implantation energies the distributions found mostly resemble a peaked shape with a tail to greater depth. In the following discussion, however, quantitative conclusions will be only drawn for Gaussian distributions, nevertheless the results will hold qualitatively for peaked shape distributions.

It can be shown, that Eq. (1) with  $\Delta R_p$  replaced by  $(\Delta R^2 + 2Dt)^{1/2}$  is a particular solution (Ref. 12) of the true diffusion equation where  $D$  and  $t$  are the diffusion coefficient and time, respectively. For  $x = R_p$  a simple relation between decrease of the relative average concentration at peak maximum and  $Dt$  value is given by

$$n(R_p, t) / n(R_p, 0) = (1 + 2Dt / \Delta R_p^2)^{-1/2}. \quad (2)$$

This equation allows a simple fit of  $D$  values for well-buried layers.

During the slowing down process of implanted ions a considerable amount of damage is produced along the track. For heavy ions this damage is more or less equally distributed along the total length of the ion track. Radiation damage, however, can effect diffusion,<sup>13</sup> and if the diffusion coefficient is different on both sides of the implanted layer, an unsymmetrical broadening may be observed. In the extreme case when diffusion only goes to one side, for example, enhanced diffusion towards the surface (cf. Fig. 4), the decrease of the peak maximum and the distribution between  $R_p$  and the surface can be described by using a higher value of the diffusion coefficient in this region as compared to that at deeper depths. The extent of the region with higher diffusion coefficient, depends on the amount and depth distribution of disorder as well as the nature of the mechanisms leading to enhanced diffusion.

For shallow implants where the peak in the distribution is of the order of some hundreds of angstroms, the influence of the surface must be considered. The case of a reflecting boundary which is impermeable to matter with the boundary condition  $\partial n / \partial x = 0$  at  $x = 0$ , the diffusion equation can be solved by adding two solutions, one placed as a mirror source of the other.<sup>14</sup> In case of outdiffusion or evaporation the rate limitation process may be due to (a) the diffusion of the implanted ions from the bulk to the surface or (b) the rate  $K$  at which the particles can cross the boundary between solid and gas.<sup>14</sup>

For a surface acting as a perfect sink we impose the condition<sup>14</sup> that the concentration is zero at  $x=0$  for all values of  $t>0$ . This boundary condition is of course only a crude approximation and may not hold in practical cases. Nevertheless, we will derive a solution for this boundary condition to get qualitative description of our results. The solution of the diffusion equation for the above boundary condition and for an initial distribution analogous to (1) is as follows:

$$n(x, t) = \frac{n(R_p, 0)}{[1 + (2Dt/\Delta R_p^2)]^{1/2}} \times \left[ \exp\left(-\frac{(x-R_p)^2}{2\Delta R_p^2 + 4Dt}\right) - \exp\left(-\frac{(x+R_p)^2}{2\Delta R_p^2 + 4Dt}\right) \right] \quad (3)$$

The decrease of the relative average concentration at  $x=R_p$  is described by

$$\frac{n(R_p, t)}{n(R_p, 0)} = \frac{1}{[1 + (2Dt/\Delta R_p^2)]^{1/2}} \times \left[ 1 - \exp\left(-\frac{4R_p^2}{2\Delta R_p^2 + 4Dt}\right) \right] \quad (4)$$

The functions (2) and (4) have been calculated and the relative decrease of the maximum concentration versus values of  $Dt/\Delta R_p^2$  is plotted in Fig. 3. Curve 1 represents the results obtained from Eq. (2), i.e., for a well-buried layer without influence of the surface. Curves 2-4 are calculated for different ratios of  $R_p/\Delta R_p$  in Eq. (4) which cover the range of measured values. The influence of the surface for values of  $Dt \geq \Delta R_p^2$  is clearly indicated. These curves were used to determine  $D$  values from measured fractional decrease in isothermal as well as in isochronal anneal sequences.

A detailed theoretical treatment<sup>7,8</sup> has been developed to determine the fractional release  $F$  of inert gases from solids in absence of trapping, where  $F = (1 - C_{\text{int}})_{x=0}$  and  $C_{\text{int}}$  is the integral of  $n(x)$  over the depth distribution. For a peaked distribution with exponential tail,  $C_{\text{int}}$  is given by<sup>7</sup>

$$C_{\text{int}} = 2y(\pi)^{1/2} + (1 - 2y^2) \exp(y^2) \operatorname{erfc} y, \quad (5)$$

with  $y^2 = Dt/R^2$ . This function had been calculated and plotted<sup>8</sup> with all ranges expressed in terms of median or 50% range  $R_m$ . This function was recalculated in terms of  $\Delta R_p^2$ , ( $R_m = 1.24R_p$ ,  $R_p = 2\Delta R_p$ ) and plotted in Fig. 3 as curve (5).

In cases where the diffusion coefficient is uniform over the entire implanted region and the surface does not present a barrier to out-diffusion, then the diffusion coefficient can be obtained from either the decrease [Eq. (5)] or the distribution [Eq. (4)] of implanted species. If there is a barrier at the surface, as has been

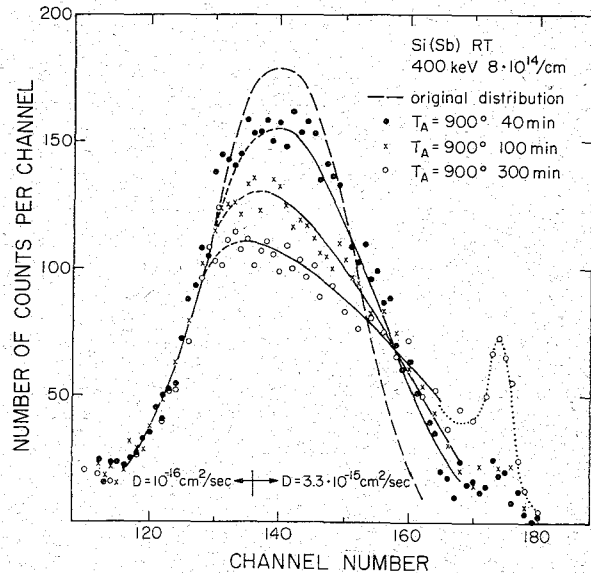


Fig. 4. Backscattered random impurity peak for a 400-keV Sb implant for different isothermal anneal times at 900°C. The dashed line represents the original distribution (see Fig. 1). The solid lines are calculated from Eq. (3) using  $D = 10^{-16}$  cm<sup>2</sup>/sec for the deeper portion of the distribution and  $D = 3.3 \times 10^{-15}$  cm<sup>2</sup>/sec for the enhanced diffusion towards the surface.

observed for Sb in Ge,<sup>15</sup> analysis of only the decrease of the number of implanted atoms will give a higher diffusion coefficient than that obtained from the changes in the distribution.

There is a case in which the shape of the distribution would not change although the integral number of atoms was decreasing. If trapping or precipitation occurred in the implanted layer and release from the centers was the rate-limiting step, out-diffusion could occur without an appreciable shift in the distribution of the remaining (trapped) atoms. This would also be found if the rate-limiting step were simple dissociation of substitutional atoms into highly mobile interstitials which could subsequently diffuse to the surface or far into the bulk before recapture.

#### IV. RESULTS

Figure 4 shows the impurity peak for a series of isothermal anneal sequences on a 400-keV Sb implantation in silicon at room temperature. The dashed curve represents the distribution of implanted Sb for the as-implanted condition. No change in distribution was found after a 15-min anneal at 800°C (see Fig. 2). In the isothermal anneal sequences, it can be seen that the distributions of Sb atoms at the lower channel numbers (i.e., at deeper depths in the crystal) are relatively unchanged during the anneal period. However, there is a decrease observed in the height of the distribution and also a broadening of the distribution towards the surface. This asymmetrical distribution is indicative of a nonconstant diffusion coefficient within the implanted layer. In order to evaluate the changes

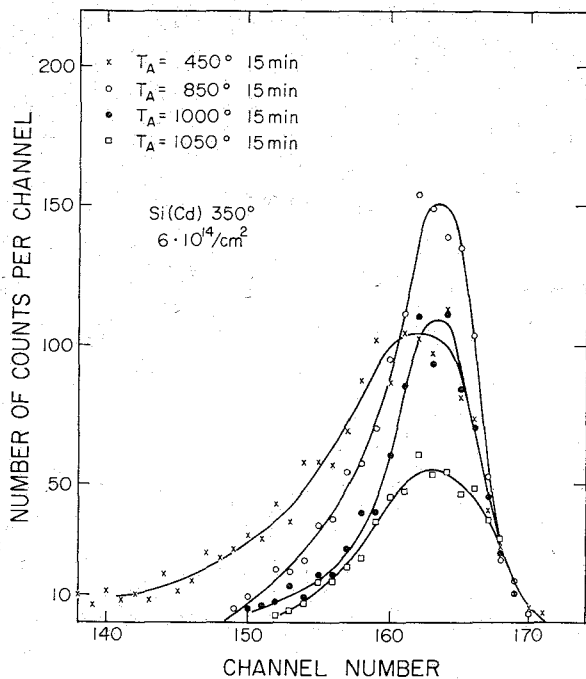


Fig. 5. Backscattered random impurity peak for a 50-keV Cd implant, 350°C substrate temperature, following 15-min anneals at four different temperatures. The original distribution coincided with the given spectrum at 450°C. The isochronal anneal sequence was carried out in 50°C steps from 450°C.

in distribution a value<sup>14</sup> of  $D = 10^{-16}$  cm<sup>2</sup>/sec was used for the deeper flank of the profile and a higher diffusion coefficient,  $D = 3.3 \times 10^{-15}$ , for the region from the peak to the surface. These values were used in Eq. (3) to determine the peak decrease and the distribution for different isothermal anneal times as shown by the solid lines in Fig. 4. The shape of the calculated impurity distribution agrees well with the experimentally determined values for all isothermal anneal times.

The integrated number of counts under the impurity peak was constant throughout the isothermal anneal sequence at 900°C. At the surface, the growth of a peak (dotted line) in the impurity distribution indicates that Sb ions have diffused to the surface and were trapped there. In the aligned spectrum obtained during these anneal sequences, it was found that those atoms at the surface were not on substitutional lattice sites and possibly were trapped at the interface between the silicon and native oxide layer.<sup>16</sup>

The fact that the Sb atoms are captured at the surface indicates that there is a barrier to their diffusion out of the sample. Similar results<sup>1</sup> had been noted earlier in the analysis of 50-keV Sb implantations.

The width of the surface peak gives an indication of the energy resolution of the detector-amplifier system. It can be seen that this resolution is much sharper than the antimony distribution. It can also be seen in Fig. 4, that the number of Sb atoms in the surface peak is a relatively small portion of the total antimony distribu-

tion. This indicates that loss of the Sb atoms to the surface played a relatively small role in determining the shape of the impurity distribution. This follows immediately from the fact that the diffusion length  $(Dt)^{1/2}$  (using the higher value of the diffusion coefficient) is less than  $\frac{1}{2}R_p$ .

Measurements on Sb-implanted samples (50 keV, RT) indicated a shift of the distribution towards the surface at temperatures near 900°C. Further isochronal anneal to higher temperatures produced a decrease in the total number of Sb atoms. At 1000°C about 50% of the Sb atoms had evaporated from the sample. No broadening of the distribution into the bulk was observed during the heat treatment. For Sb the measured activation energy required to cross the boundary between solid and the gas was about  $3.9 \pm 0.3$  eV. This value happens to be similar to the activation energy for true diffusion of Sb in Si.<sup>14</sup>

The influence of the surface can also be seen in Fig. 5 which shows the random impurity spectra for a series of anneal sequences on a sample implanted with Cd at substrate temperatures of 350°C. It can be seen that the as-implanted distributions are characterized by a peak near the surface followed by a tail. At the anneal temperature of 850°C, the impurity spectrum is shifted to the surface. At this temperature, there is no decrease in the total number of Cd atoms. The fact that the impurity spectrum shows only a shift towards the surface (i.e., to higher channel numbers) indicates that again there is an enhanced diffusion to the surface. At higher anneal temperatures there is a decrease in the

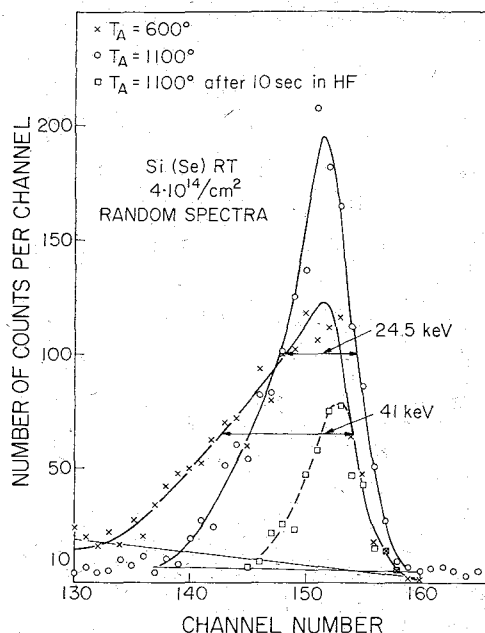


Fig. 6. Backscattered random impurity peaks for a 50-keV Se implant at RT, for 15-min isochronal anneals at 600° and 1100°C. The original distribution coincided with given spectrum at 600°C. The dashed curve is the spectrum obtained after a 10-sec HF treatment.

peak height and also in the total number of Cd ions, indicating that out-diffusion has taken place.

Se implanted in Si provides another example where a barrier is found to the out-diffusion. Channeling effect measurements indicated a 25% level of substitutional Se atoms at 600°C for RT-implanted samples. A decrease of this level to less than 5% was noted between 650° and 700°C. For samples implanted at 350°C a substitutional level of 30% was found.<sup>17</sup> This level increases to 40% with increasing temperature up to 900°C and then decreases. In both cases the decrease of the substitutional level was connected with a motion of the Se atoms towards the surface and precipitation at the surface. The influence of the barrier at the surface for a RT implant is shown in Fig. 6. The random spectrum following an isochronal anneal at 1100°C is both shifted towards the surface and narrowed. The total number of counts in the impurity spectrum is unchanged. The spectrum taken after a 10-sec dip in HF (dashed line) showed that more than  $\frac{3}{4}$  of the Se atoms had been removed. This indicates that Se atoms were trapped near the Si-SiO<sub>2</sub> interface.

A case where the surface did not present an appreciable barrier to the out-diffusion of the implanted atoms is shown in Fig. 7 for a sample implanted with I at room temperature. In this case, the spectra did not show an appreciable shift to the surface and no decrease in width was observed during 15-min isochronal anneal periods.

The anneal of lattice disorder can also have a large influence on the out-diffusion of implanted species. Figure 8 shows the integral number of Zn and Cd atoms as the function of isochronal anneal temperature for

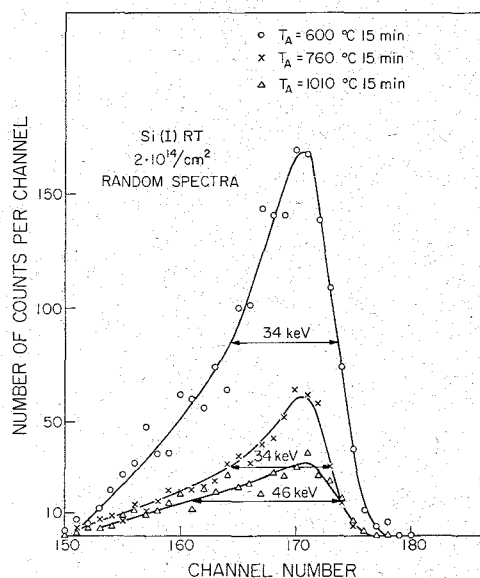


FIG. 7. Backscattered random impurity peaks for a 50-keV I implant at RT after 15-min isochronal anneal steps at 600° (O), 760° (X), and 1010°C (Δ). In this sample the reordering of the lattice occurred above 600°C.

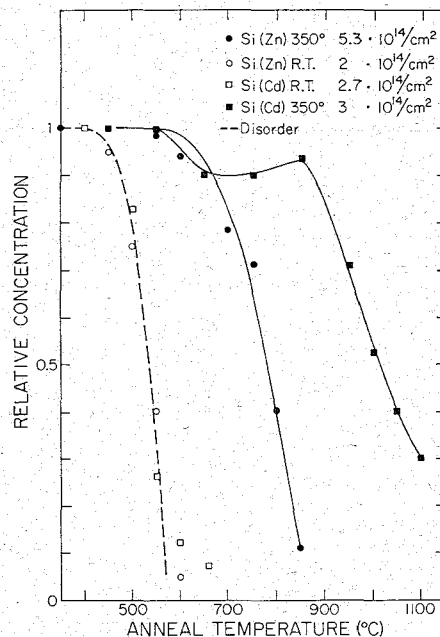


FIG. 8. Relative number of atoms per cm<sup>2</sup> as a function of 15-min isochronal anneals for 50-keV Zn and Cd implants at RT and 350°C substrate temperature.

implantation at room temperature and substrate temperatures of 350°C.

For the room-temperature implantations an amorphous layer was formed (see Fig. 1 for the Zn case). The anneal of the disorder is shown by the dashed line in Fig. 8. Both the Zn- and Cd-implanted layers showed a decrease in the number of atoms that coincided closely with the reordering of the amorphous layer. For these RT implants, there was neither an apparent sticking at the surface, nor a broadening into the bulk as can be seen from the Zn spectra in Fig. 1. In this mixed implant both the decrease of the total number of Zn atoms and the decrease of disorder was shifted by about 50°C to temperatures compared with the results presented in Fig. 8. This again shows that the out-diffusion of Zn is closely connected with the anneal of disorder.

For the implantation at 350°C, the decrease in both the number of Zn and Cd atoms occurred at significantly higher temperatures than in the room-temperature implantation. In the as-implanted condition at 350°C there were approximately 30%–40% of the Zn and Cd atoms on the tetrahedral interstitial sites.<sup>17</sup> During isochronal anneal the Zn atoms were observed<sup>17</sup> to move from interstitial sites to "nonregular" lattice positions (possibly precipitation sites) at temperatures near 550°–600°C. For Cd this motion from interstitial sites occurred around 650°C. It should be noted that the out-diffusion observed for Zn occurred at temperatures above that where the interstitial species moved off lattice sites. For the cadmium case, the shift towards the surface occurred in the same temperature range as

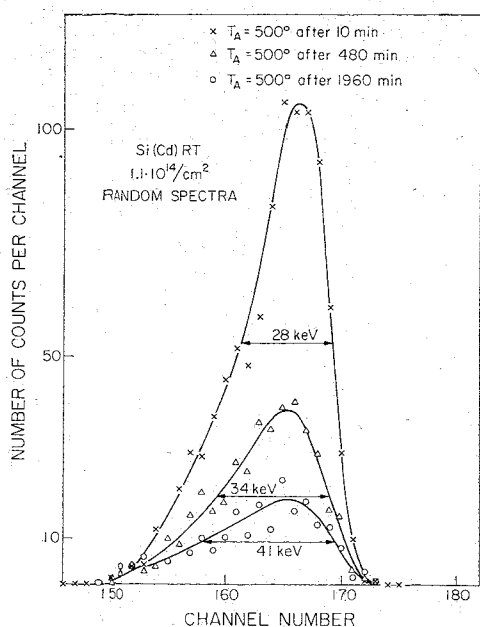


Fig. 9. Backscattered random impurity peaks for a 50-keV Cd implanted at RT after three isothermal anneal sequences at 500°C.

the motion from interstitial sites and there was an apparent barrier to the out-diffusion (as noted in Fig. 5).

The out-diffusion observed in the room-temperature Cd-implanted samples was studied in greater detail in isothermal anneal sequences. Random impurity spectra for a room-temperature 50-keV Cd implant are shown in Fig. 9. It can be seen that the peak decreases with increased anneal time and that there is no apparent broadening of the distribution deeper into the silicon. Further, there is no appreciable shift to the surface during annealing. This is different from the results noted on the 350°C implantation shown in Fig. 5. The integrated number of Cd ions and the amount of lattice disorder as a function of isothermal anneal time at 500°C is shown in Fig. 10. From this curve it can be seen that the out-diffusion of the Cd lagged somewhat behind the anneal of the lattice disorder. The diffusion coefficient at 500°C, calculated from the decrease in the average peak concentration was  $D = 2.5 \times 10^{-16}$  cm<sup>2</sup>/sec. From the isochronal anneal data decrease of the average peak concentration with diffusion coefficient extrapolated to 500°C was  $5 \times 10^{-16}$  cm<sup>2</sup>/sec, and from the decrease of the total number (Fig. 8)  $D$  was  $10^{-15}$  cm<sup>2</sup>/sec. These differences may reflect the different assumptions used in the calculations.

For other species the out-diffusion observed in room-temperature-implanted species may not be connected with the reordering of the amorphous layer. For example, this connection is not observed at these temperatures in Si samples implanted with group III and V species.<sup>3</sup> In this work, it was found that the out-diffusion of Rb, Cs, Se, and Te occurred at temperatures above that where the amorphous layer reordered. The

decrease in the number of Rb and Cs atoms/cm<sup>2</sup> as a function of isochronal anneal temperature is shown in Fig. 11.

In samples implanted at RT the decrease in the number of atoms (solid line) was shifted to temperatures significantly higher than that at which the amorphous layer reordered (dashed line). For the case of Rb the decrease is shifted 100°–150°C higher than that for the reordering of the lattice. For Cs, Se, Te, and Sb, negligible out-diffusion was found in the temperature region where the amorphous layer reorders. This is shown in Fig. 11 for the case of Cs. For Cs implanted samples at doses between  $8 \times 10^{13}$  and  $5 \times 10^{14}$  ions/cm<sup>2</sup> the major decrease in the number of implanted atoms occurs between 1000° and 1150°C.

In samples implanted with Rb and Cs at 350°C, the aligned silicon spectrum indicated that most of the disorder annealed during implantation. However, there was some decrease in the Rb content at the anneal temperature at which out-diffusion occurred in the room-temperature-implanted samples. The major portion of the decrease occurred at temperatures above 900°C. In all cases and throughout the entire anneal range, there was no indication that Rb or Cs occupied regular lattice sites.

## V. DISCUSSION

In the annealing behavior of implanted species of silicon, we have noted three major effects which can influence the out-diffusion of implanted species: (1) enhanced diffusion to the surface, (2) retardation or sticking at the surface, and (3) reordering of the amorphous layer. The data also suggest that release of atoms from trapping (precipitation) sites in the implanted layer can be the rate-limiting process in some cases.

The presence of enhanced diffusion towards the surface was shown most clearly in the impurity distributions measured on the sample implanted with Sb at 400 keV (Fig. 4). The effective diffusion coefficient was

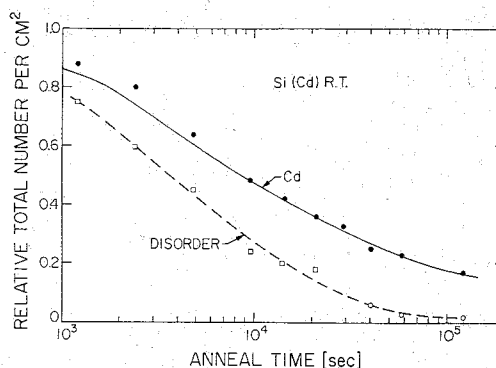


Fig. 10. The amount of lattice disorder and the total of the implanted Cd atoms/cm<sup>2</sup> in the impurity peak (Fig. 9) versus time for isothermal anneal at 500°C. The solid line was calculated (Fig. 3, curve 2) for  $D = 2.5 \times 10^{-16}$  cm<sup>2</sup>/sec.

33 times that given<sup>14</sup> for thermal diffusion of Sb at 900°C. Enhanced diffusion to the surface is also indicated by the narrowing and shift of the distribution found in the Se (Fig. 6) and Cd (Fig. 7) implants. Channeling effect data indicated that the Sb and Se were on substitutional sites and much of the lattice disorder had annealed before the motion towards the surface occurred. The mechanism responsible for enhanced diffusion towards the surface is not clear at present. It cannot be attributed to the boundary condition at the surface. One might speculate that it is caused by residual disorder in the implanted layer or the motion of dislocations to the surface. The presence of dislocations in implanted samples has been well established. Note, however, that the motion of Se occurred at 650°C and that of Sb at 900°C.

For all three cases (Sb, Se, and Cd) the presence of a barrier at the surface was evident. Channeling effect data indicated that the Sb and Se atoms located near the surface were displaced off regular lattice sites. Stripping measurements in this (Fig. 6) and previous work<sup>1</sup> indicated that the atoms are located near the Si-SiO<sub>2</sub> boundary. In 50-keV implanted samples, the decrease in the total number of Sb and Cd (at anneal temperatures higher than that where trapping occurred) could be analyzed in a fashion similar to that used in gas-release data in order to determine diffusion parameters. In this case, however, the rate-limiting process would be the motion away from the interface (evaporation) rather than diffusion in the implanted layer.

The correlation between the reordering of the amorphous layer and decrease in the total number of implanted atoms was clearly established for Zn and Cd RT implants (Figs. 8 and 10). Similar results were also found for I and Hg implants. Further indication that such a correlation exists is found in the mixed Zn and Bi implants where *both* disorder anneal and out-diffusion of Zn were shifted 50° higher than the case for Zn alone.

The mechanism responsible for this correlation is not yet obvious. When an amorphous layer reorders it has earlier been shown that recrystallization starts at the interface between Si crystal and disorder.<sup>2</sup> This could suggest that the implanted species are swept out in a manner analogous to zone refining. This would produce a sharpening and shift towards the surface. As one can see from the Zn peak in Fig. 1 such effects are not found. The decrease in width of the Si surface peak is nearly a factor of 2, whereas the Zn peak width remains nearly constant. The correlation is not simply due to the fact that the diffusion constant is lower in the amorphous region. This would produce a broadening of the distribution into the bulk which was not found. There is also the fact that Rb, implanted at RT, out-diffuses after the amorphous layer reorders but the amount of the decrease is significantly different than that found for 350°C implants (Fig. 11).

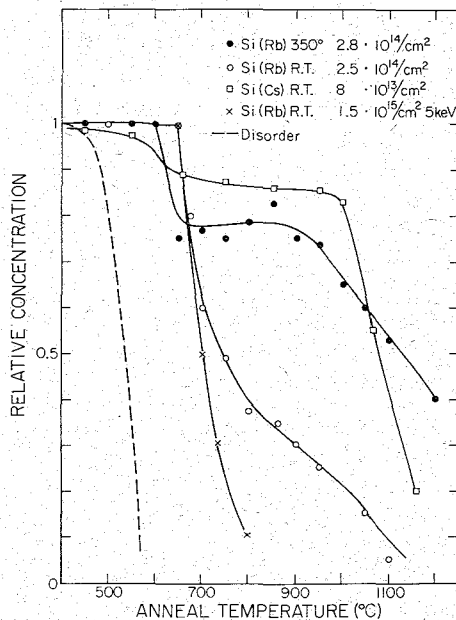


Fig. 11. Relative number of atoms/cm<sup>2</sup> versus a 15-min isochronal anneal for 50-keV Rb implanted at RT and 350°C, 50-keV Cs implanted at RT and 5-keV Rb implanted at RT. The dashed curve represents the anneal of the disorder in RT implanted Rb and Cs samples.

The fact that there is no shift in the distribution while the integral number of the peak was decreasing suggests that the release of atoms from trapping (precipitation) sites<sup>18</sup> in the implanted layer can be the rate limiting<sup>19</sup> process. This point is supported in the 350°C Zn implants in which the interstitial Zn moves to nonregular lattice sites about 200°C before a peak decrease is noted. It is possible the observed decrease of the number of atoms in the peak is not entirely due to out-diffusion alone. Diffusion into the bulk is possible if, after release from traps, the diffusion length  $(Dt)^{1/2}$  is much greater than  $\Delta R_p$ . Here one would expect a broad tail in the backscattering spectra extending to lower energies. We did not observe this. However, if the concentration of the tail of the diffused species was less than 1% of the average peak concentration, this level would be below the sensitivity of the backscattering measurement. In this case we could not distinguish (in our experimental procedure) between the case for out-diffusion *and* in-diffusion and that for out-diffusion alone. For example, the effective diffusion coefficient for 350°C Zn implants at 700°C (which, of course could be dominated by release from traps) determined by the decrease in the average peak concentration is about two orders-of-magnitude lower than the extrapolated value<sup>19</sup> of the diffusion coefficient in bulk material.

It should be noted that a decrease in the number of implanted atoms may not be due to diffusion effects only. It is possible that some of the underlying substrate might be removed during anneal treatment. This could be a major effect in compound semiconductors where

the vapor pressure of one of the constituents can be high enough to cause dissociation during thermal processing. This consideration may not be restricted to compound semiconductors. Preliminary measurements by Johansson and Sigurd<sup>20</sup> indicate that heat treatment causes removal of surface layers of Ge. So far, this has been noted for anneal temperatures greater than 600°C.

## VI. CONCLUSIONS

The diffusion effects noted in implanted silicon are complicated and the mechanisms leading to out-diffusion behavior are not obvious. It is clear that measurement of only the decrease of the total number of implanted atoms, a procedure similar to that used in gas-release studies, is not sufficient to determine diffusion coefficients and activation enthalpies. A necessary first step is to determine both the amount of disorder and the shape of the impurity distribution. In order to connect the diffusion coefficient found for implanted layers with true bulk diffusion, it is necessary to find cases in which the distribution broadens into the crystal as well as to the surface. Even here it still may not be possible to connect these diffusion coefficients since enhanced diffusion *into* the crystal has been observed.<sup>13</sup>

Elastic scattering and channeling effect measurements are useful tools in the analysis of diffusion effects in implanted semiconductors. From the backscattering spectrum obtained for random orientation, it is possible to determine both the total number of implanted atoms and their depth distribution. The effective diffusion coefficient can be obtained directly from either the shift in the distribution or the decrease in the number of implanted atoms or the height of the impurity peak. The aligned spectra are used to obtain the amount of lattice disorder and hence can be used to correlate out-diffusion effects and the reordering of the disordered regions. The aligned spectra are also useful to determine the lattice location (substitutional, interstitial) of the implanted species and to determine if motion

off lattice sites occurs before or during the out-diffusion process.

## ACKNOWLEDGMENTS

The authors acknowledge with pleasure discussions with J. Gyulai and S. T. Picraux. The implantations were performed at the Research Institute for Physics, Stockholm, Physics Dept., Aarhus (400-keV Sb), and Institute for Applied Nuclear Physics (Nuclear Research Center), Karlsruhe.

\* Supported in part by A. F. Cambridge Research Laboratories, National Science Foundation (GP-9114) and the Office of Naval Research [Nonr-220(47)].

† Permanent address: Institut für Angewandte Kernphysik, Kernforschungszentrum Karlsruhe, Germany.

<sup>1</sup> J. A. Davies, J. Denhartog, L. Eriksson, and J. W. Mayer, *Can. J. Phys.* **45**, 4073 (1967).

<sup>2</sup> J. W. Mayer, L. Eriksson, S. T. Picraux, and J. A. Davies, *Can. J. Phys.* **46**, 663 (1968).

<sup>3</sup> L. Eriksson, J. A. Davies, N. G. E. Johansson, and J. W. Mayer, *J. Appl. Phys.* **40**, 842 (1969).

<sup>4</sup> R. F. Sippel, *Phys. Rev.* **115**, 1441 (1959).

<sup>5</sup> S. T. Picraux, N. G. E. Johansson, and J. W. Mayer, in *Semiconductor Silicon*, edited by R. R. Haberecht and E. L. Kern (Electrochemical Society, New York, 1969), p. 422.

<sup>6</sup> C. Jech and R. Kelly, *J. Phys. Chem. Solids* **30**, 465 (1969).

<sup>7</sup> R. Kelly and H. J. Matzke, *J. Nucl. Mater.* **20**, 171 (1966).

<sup>8</sup> H. J. Matzke, *Z. Naturforsch.* **22a**, 507 (1967).

<sup>9</sup> For a review on gas-release work up to 1967 see for example G. Carter and J. S. Colligon, *Ion Bombardment of Solids* (Elsevier, New York, 1968).

<sup>10</sup> F. M. Smits and R. C. Miller, *Phys. Rev.* **104**, 1242 (1956).

<sup>11</sup> J. Halpern and R. H. Rediker, *Proc. IRE* **46**, 1068 (1958).

<sup>12</sup> T. E. Seidel and A. U. MacRae, *Trans. AIME* **245**, 491 (1969).

<sup>13</sup> P. Baruch and J. Pfister, *Radiation Damage in Solids* (International Atomic Energy Agency, New York, 1963), Vol. 3, p. 43.

<sup>14</sup> B. I. Boltaks, *Diffusion in Semiconductors* (Academic, New York, 1963).

<sup>15</sup> R. C. Miller and F. M. Smith, *Phys. Rev.* **107**, 65 (1957).

<sup>16</sup> Channeling effect measurements on samples after implantation indicated that the oxide layer was about 20–30-Å thick.

<sup>17</sup> J. Gyulai, J. W. Mayer, and O. Meyer (unpublished).

<sup>18</sup> Another similar mechanism is simple dissociation of substitutional atoms into interstitials. However, Zn was not found on substitutional sites and hence the dissociation mechanism is probably not applicable for this case.

<sup>19</sup> D. L. Kendall and D. B. DeVries, in Ref. 5, p. 358.

<sup>20</sup> N. G. Johansson and D. Sigurd (unpublished).



